

The Influence of Atlantic Variability on Asian Summer Climate Is Sensitive to the Pattern of the Sea Surface Temperature Anomaly

SATYABAN B. RATNA, TIMOTHY J. OSBORN, AND MANOJ JOSHI

Climatic Research Unit, School of Environmental Sciences, University of East Anglia, Norwich, United Kingdom

JÜRIG LUTERBACHER

Department of Geography, Climatology, Climate Dynamics and Climate Change, and Centre of International Development and Environmental Research, Justus Liebig University Giessen, Giessen, Germany, and World Meteorological Organization, Science and Innovation Department, Geneva, Switzerland

(Manuscript received 21 January 2020, in final form 28 April 2020)

ABSTRACT

We simulate the response of Asian summer climate to Atlantic multidecadal oscillation (AMO)-like sea surface temperature (SST) anomalies using an intermediate-complexity general circulation model (IGCM4). Experiments are performed with seven individual AMO SST anomalies obtained from CMIP5/PMIP3 global climate models as well as their multimodel mean, globally and over the North Atlantic Ocean only, for both the positive and negative phases of the AMO. During the positive (warm) AMO phase, a Rossby wave train propagates eastward, causing a high pressure and warm and dry surface anomalies over eastern China and Japan. During the negative (cool) phase of the AMO, the midlatitude Rossby wave train is less robust, but the model does simulate a warm and dry South Asian monsoon, associated with the movement of the intertropical convergence zone in the tropical Atlantic. The circulation response and associated temperature and precipitation anomalies are sensitive to the choice of AMO SST anomaly pattern. A comparison between global SST and North Atlantic SST perturbation experiments indicates that East Asian climate anomalies are forced from the North Atlantic region, whereas South Asian climate anomalies are more strongly affected by the AMO-related SST anomalies outside the North Atlantic region. Experiments conducted with different amplitudes of negative and positive AMO anomalies show that the temperature response is linear with respect to SST anomaly but the precipitation response is nonlinear.

1. Introduction

Sea surface temperatures (SST) in the North Atlantic Ocean exhibit multidecadal fluctuations (Schlesinger and Ramankutty 1994; Delworth and Mann 2000; Zhang and Delworth 2005; Ghosh et al. 2016; Wang et al. 2017; O'Reilly et al. 2019) that are commonly expressed as the Atlantic multidecadal oscillation (AMO). The AMO

is a basin-scale SST variation in the North Atlantic characterized by alternating basin-scale warming and cooling with an apparent period of 65–80 years and an amplitude of 0.4°C during the instrumental period (Kerr 2000; Enfield et al. 2001). Variability in the North Atlantic Ocean occurs because of both internal processes (Delworth et al. 1993; Knight et al. 2005) and external forcings such as volcanic, solar, and anthropogenic effects (Cubasch et al. 1997; Otterå et al. 2010; Chylek et al. 2011; Knudsen et al. 2011; Booth et al. 2012; Wang et al. 2017). The AMO is sometimes referred to as the internally generated component of Atlantic multidecadal variability (AMV) and is the largest contributor to the AMV (Wang et al. 2017; Coats and Smerdon 2017), whereas

 Denotes content that is immediately available upon publication as open access.

 Supplemental information related to this paper is available at the Journals Online website: <https://doi.org/10.1175/JCLI-D-20-0039.s1>.

Corresponding author: Satyaban B. Ratna, s.bishoyi-ratna@uea.ac.uk



This article is licensed under a [Creative Commons Attribution 4.0 license](http://creativecommons.org/licenses/by/4.0/) (<http://creativecommons.org/licenses/by/4.0/>).

other studies use the two terms synonymously (Keenlyside et al. 2016).

The AMO primarily reflects internal variability associated with the Atlantic meridional overturning circulation (Zhang and Delworth 2005; Sutton and Hodson 2005; Knight et al. 2006; Ting et al. 2011). SST variations are related to ocean density anomalies in deep water formation regions of the North Atlantic and associated ocean heat transport fluctuations (Folland et al. 1986; Gray et al. 1997; Delworth and Mann 2000; Knight et al. 2005; Msadek et al. 2011; Zhang and Wang. 2013). The AMO contributes to multidecadal fluctuations in the global-mean surface temperature (Kajtar et al. 2019) and exerts significant influences on monsoons in different parts of the globe (Trenberth et al. 2000; An et al. 2015; Monerie et al. 2019). Both observational and climate model studies have shown that the AMO affects climate in regions such as North America (Schubert et al. 2004; McCabe et al. 2004; Sutton and Hodson 2005; Feng et al. 2011; Oglesby et al. 2012; Hu and Veres 2016) and Europe (Sutton and Hodson 2005; Ghosh et al. 2016) and impacts on Atlantic hurricane frequency (Goldenberg et al. 2001; McCabe et al. 2004; Zhang and Delworth 2006), Sahel rainfall (Zhang and Delworth 2006) and spring precipitation in northeastern Brazil (Knight et al. 2006).

The AMO may also influence East Asian climate in summer (Lu et al. 2006; Li and Bates 2007; Liu and Chiang 2012; Xia et al. 2013; Li and Luo 2013; Gao et al. 2014; Qian et al. 2014; Si and Ding 2016; Zhu et al. 2016) and winter (Li and Bates 2007; Sun et al. 2012). Wang et al. (2009) found that the influence of AMO favoring warmer temperature in East Asia exists in all seasons of the year. Multidecadal variability in heat-wave events over eastern China has also been attributed to the AMO (Xia et al. 2016). Apart from the instrumental data and modeling studies discussed above, a relationship between East Asian temperature and the AMO has also been suggested in past climate studies using paleoclimatic evidence (Li et al. 2015; Wang et al. 2013, 2014; Fang et al. 2019). The AMO influences East Asia by the propagation of Rossby waves (Knight et al. 2005; Li and Bates 2007; Li et al. 2008; Grossmann and Klotzbach 2009; Luo et al. 2011), which can extend all the way to North America (Si and Ding 2016). The AMO also affects the East Asian summer (Zhang et al. 2018) and winter monsoons (Hao and He 2017) by altering the interhemispheric thermal contrast (Dong et al. 2006; Wang et al. 2009).

Several observational and modeling studies suggest that the AMO influences South Asian climate, particularly the Indian summer monsoon (ISM): a positive or negative AMO phase respectively corresponds to a

strengthening or weakening of the ISM (Zhang and Delworth 2005; Goswami et al. 2006; Li et al. 2008; Wang et al. 2009; Msadek and Frankignoul 2009). Goswami et al. (2006), Luo et al. (2011), and Lu et al. (2006) found that a warm phase of the AMO causes a late withdrawal of the ISM and hence enhanced seasonal rainfall. Other studies suggest that any AMO influence on rainfall within India during the ISM varies between regions (Knight et al. 2006; Lu et al. 2006; Zhang and Delworth 2006; Wang et al. 2009). The AMO–ISM teleconnections may extend back to the past two millennia (Feng and Hu 2008) and earlier in the Holocene (Gupta et al. 2003; Fleitmann et al. 2003). It has also been found that the ISM can have a remote impact on the variability of East Asian climate through atmospheric teleconnection patterns forced by diabatic heating associated with the monsoon (Hoskins and Rodwell 1995; Ding and Wang 2005; Greatbatch et al. 2013).

It has been suggested that the AMO can change the meridional temperature gradient between the Asian continent and the tropical Indian Ocean, which then influences the intensity of the ISM (Goswami et al. 2006; Lu et al. 2006; Feng and Hu 2008; Wang et al. 2009; Luo et al. 2011; Msadek et al. 2011). Zhang and Delworth (2006) suggested that the warm AMO in their model leads to a northward shift of the intertropical convergence zone (ITCZ) and surface southwesterly anomalies over the Sahel and India and consequently a stronger ISM. Li et al. (2008) suggested that warm extratropical North Atlantic SSTs increase local rainfall, inducing an extratropical wave train response. The latter leads to intensified northern subsidence of monsoon mean meridional streamflow as well as widespread low surface pressure over North Africa, the Middle East, and the western Indian Ocean contributing to a strengthened Indian monsoon trough and increased monsoon rainfall. Another possible mechanism linking the Atlantic region with Asian monsoons is through air–sea interactions, in which a positive AMO leads to warm SST responses in the Indo-Pacific region (Dong et al. 2006; Zhou et al. 2015; Sun et al. 2017) and an anomalous easterly wind response in the equatorial western Pacific Ocean. This intensifies the land–sea thermodynamic contrast and causes an enhanced ISM. Luo et al. (2011) suggested that the consistency between uncoupled atmospheric models and coupled climate models for the relationship for AMO–ISM suggests that atmospheric dynamical processes play the most important role.

In summary, recent work shows that the AMO is a significant source of variability for Asian climates but the effects vary seasonally, among regions, and also among models; limitations of observational datasets also leave considerable uncertainty. Furthermore, Ratna et al. (2019)

highlight the potentially confounding effects of external forcing when evaluating AMO–Asia teleconnections and that different GCMs produce quite different Asian responses to the AMO. Previous literature focused on how different AMO phases relate to climate responses over different parts of the globe. However, there has not been an investigation of how different AMO SST patterns affect the climate response over South and East Asia. So, we have designed atmospheric model experiments to understand the response to different AMO-like SST patterns over the North Atlantic on the South and East Asia climate.

We formulate the following research questions:

- (i) Different coupled GCMs simulate different linkages between AMO and South and East Asia: is this because they simulate different AMO SST anomaly patterns (in either the North Atlantic or elsewhere)?
- (ii) Do the opposite phases of the AMO (AMO+ and AMO–) result in different responses of circulation, temperature, and precipitation over South and East Asia in summer?
- (iii) Is the annual and seasonal temperature and precipitation response over South and East Asia linear with respect to the sign and amplitude of SST forcing?

To answer these questions, we used the AMO SST patterns (see section 2 for more details) diagnosed by Ratna et al. (2019) from seven CMIP5 models to force the intermediate-complexity general circulation model (IGCM4) atmospheric model (Joshi et al. 2015) to understand how the AMO induces the seasonal temperature and precipitation responses over South and East Asia (SEA). Section 2 outlines the model, data, and method. Section 3 compares the CMIP5 and IGCM4 simulations of the SEA surface temperature response to AMO. The spatial patterns of SEA temperature, precipitation response to AMO and the related mechanisms are discussed in section 4. The area-averaged South and East Asian monsoon responses to AMO and related mechanisms are discussed in section 5 and the nonlinearity of these area-averaged responses is considered in section 6. The conclusions are presented in section 7.

2. Data, model, and experimental design

a. CMIP5 SST data

In this study we use composited SST fields of AMO events based on the study by Ratna et al. (2019), who used seven CMIP5 models (BCC, CCSM4, MPI, HadCM3, MRI, IPSL, and CSIRO; see their Table 1 for model details) covering the period CE 850–2000. As in their study, the AMO index is the area-weighted North Atlantic (0° – 65° N, 80° W– 0°) monthly mean SST

anomaly (SSTA) calculated after subtracting the global-mean SST anomaly time series. The influence of any residual long-term drift or anthropogenic transient forcing is minimized by first removing the linear trend from the time series. The data are then passed through a 30-yr low-pass filter to isolate multidecadal variability [see Ratna et al. (2019) for details].

Composites of SST anomalies are constructed using years when the AMO index is higher or lower than 1 standard deviation, respectively denoted AMO+ and AMO– and shown in Fig. 1. The composite AMO+ SST patterns for the individual models (Figs. 1a–g) and the multimodel mean (Fig. 1h) show the different SST patterns. The multimodel mean (Fig. 1h) is dominated by positive SST in the North Atlantic, but also an association with warm SSTs extending into the Atlantic sector of the Arctic (enhanced near the sea ice edge) and with warm SSTs in the North Pacific (with a spatial structure similar to the PDO). It is linked with negative SSTA in almost all the Southern Hemisphere, perhaps indicative of enhanced heat transport from the Southern Hemisphere (SH) to the Northern Hemisphere (NH) during AMO+ phases. All main regions of warm and cool anomalies are statistically significant.

Similarly, the composite AMO– SST patterns for the individual models (Figs. 1j–p) and the multimodel mean (Fig. 1q) show a diversity of SST patterns. The multimodel-mean AMO– SST pattern (Fig. 1q) shows the opposite sign of the AMO+ in many locations, but with different amplitude in some regions. The zero anomaly line is close to 40° S for the AMO– composite (Fig. 1q) but is in the NH for the AMO+ composite, a striking difference that could affect the response of the ITCZ to tropical SST gradients. This contrast between the AMO+ and AMO– composites may partly reflect the association between periods of strong volcanic forcing and AMO– conditions, though we have reduced this affect by creating composites using an AMO index with the global-mean SST subtracted (Ratna et al. 2019).

The intermodel spread (indicated by the standard deviation; Figs. 1i,r) highlights model differences in the amplitude and location of SSTA in the North Atlantic as well as differences in the Southern Ocean SSTA. North Atlantic SSTA > 0.1 K are confined to a smaller region in the BCC (Fig. 1a) and MRI (Fig. 1e) models, whereas in the other models these warm anomalies are more extensive (either spreading farther north or south or both). This is reflected in the area-mean North Atlantic SSTA, which show the smallest differences between AMO+ and AMO– composites for the BCC (Figs. 1a,j) and MRI (Figs. 1e,n) models. The largest differences between AMO+ and AMO– composites are for the

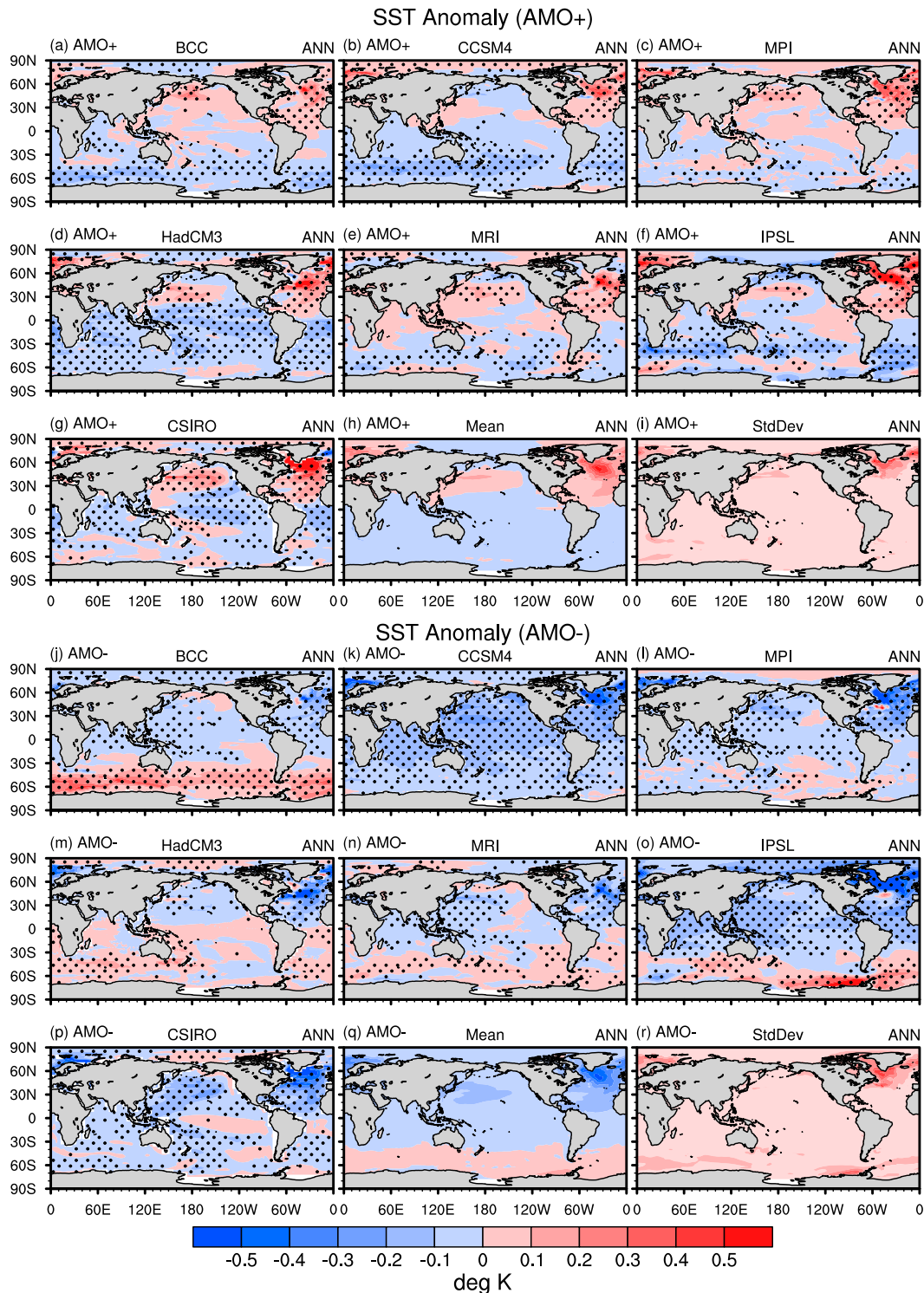


FIG. 1. Composite annual-mean SST anomaly (K) for AMO events obtained from seven CMIP5 models (BCC, CCSM4, MPI, HadCM3, MRI, IPSL, and CSIRO) for (a)–(g) AMO+ events and (j)–(p) AMO– events. The stippling shows where the individual model composites are significant (at 90% level) using a Student’s t test. Also shown are the mean SST of seven models for (h) AMO+ and (q) AMO– events and the intermodel standard deviation for (i) AMO+ and (r) AMO– events. The values and the corresponding color labels for the standard deviation are from 0 to >0.5 K.

CSIRO (Figs. 1g,p) and IPSL (Figs. 1f,o) models. The CCSM4 (Figs. 1b,k) model shows the greatest asymmetry between AMO+ and AMO−, being among the least warm for AMO+ but second coolest for AMO−. CCSM4 is also the only model to show near-global cooling during its AMO− events (Fig. 1k). Other models show strong warming in parts of the Southern Ocean during their AMO− phases (Figs. 1j,m,o) and this diversity raises the intermodel spread there (Fig. 1r). There is also diversity in the Southern Ocean SSTA for the AMO+ composites, although with reduced magnitude.

b. IGCM4 model

The IGCM4 (Joshi et al. 2015) is a global spectral primitive equation climate model whose predecessors have extensively been used in climate research, process modeling, and atmospheric dynamics (van der Wiel et al. 2016; O'Callaghan et al. 2014). IGCM4 has a spectral truncation of T42 (and a 128×64 horizontal grid) and 20 layers in the vertical direction (from the surface to 50 hPa) denoted as T42L20, which is the standard configuration for studies of the troposphere and climate. For information about the physical parameterization schemes used in this model, refer to Joshi et al. (2015). The IGCM differs from CMIP5 GCMs in that its convection scheme, based on the Betts–Miller convection scheme, is simpler than most CMIP5 GCMs (see Joshi et al. 2015; Forster et al. 2000). Large-scale clouds are handled by a relative humidity-based scheme (Slingo 1987). The surface–atmosphere exchange schemes are stability based (Forster et al. 2000) and simpler than in some CMIP5 GCMs. The soil model is a two-layer bucket model, and there is no model for canopy absorption (Forster et al. 2000). The IGCM4 gives a good representation of the mean state, which, for instance, is comparable to CMIP5 GCMs for precipitation (Figs. 4 and 5 of Joshi et al. 2015).

c. Experimental design

Climatological SSTs in the IGCM are obtained from the NOAA/Earth System Research Laboratories Twentieth Century Reanalysis, version 2 (20CRv2; Compo et al. 2011), for the period 1871–1920; this IGCM4 simulation is denoted CTRL. We used the standard configuration mixing ratios as given in Joshi et al. (2015). The model-simulated climatology in comparison with the reanalysis climatology and the details can be found in the supplemental text section and Fig. S1 of the online supplemental material).

Each of the composite SSTA patterns (Fig. 1) was multiplied by 2 [similar to the method of Monerie et al. (2019)] to strengthen the signal-to-noise ratio and added

to the 20CR climatology to provide the forcing for an IGCM simulation. All other boundary conditions were the same as in CTRL. The surface albedo was adjusted to indicate the presence or absence of sea ice according to whether the new surface temperature was below freezing. These eight experiments (seven individual SSTA patterns and the multimodel-mean SSTA) with AMO+ and eight with AMO− SST anomalies are referred to here as AMO_{glo}+ and AMO_{glo}−, respectively. To understand whether the climate response comes from the North Atlantic or elsewhere, we conducted a parallel set of experiments by adding the AMO SST anomaly over the North Atlantic only, denoted AMO_{atl}+ and AMO_{atl}−, respectively. The notations of all of the SST forced experiments are

- 1) AMO_{glo}+: 20CR SST plus $2 \times$ AMO+ global SSTA,
- 2) AMO_{glo}−: 20CR SST plus $2 \times$ AMO− global SSTA,
- 3) AMO_{atl}+: 20CR SST plus $2 \times$ AMO+ SSTA only over the North Atlantic and Arctic, and
- 4) AMO_{atl}−: 20CR SST plus $2 \times$ AMO− SSTA only over the North Atlantic and Arctic.

Last, we test the linearity of the climatic response to the AMO by performing additional experiments with a magnitude from 1 ($1 \times$) to 5 times ($5 \times$) the AMO SST anomaly (hereinafter $1 \times$ SST– $5 \times$ SST) for both positive and negative phases of AMO. These linearity experiments use only MEANsst, which is the mean of SSTA from seven CMIP5 models, and the SST anomaly applied to the North Atlantic only (same as AMO_{atl}+ and AMO_{atl}−).

For each simulation, the model is integrated for 55 years and the mean of the last 50 years is analyzed (the first 5 years are excluded to allow model spinup). We focus on the boreal summer (May–September) climatology because South and East Asia experience maximum temperature and rainfall during this season. However, some results are also given for annual or boreal winter when needed to illustrate seasonally dependent responses. We have analyzed the impact of the AMO SSTA patterns by subtracting the final 50-yr mean of the CTRL simulation from the 50-yr mean of each experiment simulation.

3. Comparing CMIP5 and IGCM Asian temperature responses to the AMO

Ratna et al. (2019) showed that the AMO was positively correlated with surface air temperatures over South and East Asia during the last millennium period, but that this relationship is not stationary in time and space between the seven CMIP5 models analyzed. These intermodel variations arise from differences in

each models' AMO-related SST pattern (Fig. 1, all panels) and from differences in each models' dynamical response to the SST. Figure 2a illustrates these different behaviors for the AMO+ composite in the CMIP5 models themselves. Figure 2b shows that IGCM4, when forced by the same SSTA patterns, is able to simulate an overall warming of annual-mean temperature in this region in response to AMOglo+ forcing. Some model-specific behavior (e.g., the contrast between warming north of 25°N and cooling south of that in HadCM3 and CSIRO) is also reproduced, suggesting that the strong north-south gradient may arise from the structure of the SSTA itself and that IGCM4's dynamical response to the SSTA is similar to those CMIP5 models. However, IGCM4 simulates a strong north-south gradient in response to the IPSL AMOglo+ SSTA but the IPSL CMIP5 model itself has no latitudinal gradient and only a weak association between Asian temperature and its positive AMO phase (Figs. 2a,b). This indicates a different dynamical response between IPSL and IGCM4. A similar conclusion is found for the BCC model, though this could partly arise from the weaker SST anomaly for that model noted earlier.

The differences between the AMOglo+ (Fig. 2b) and AMOatl+ (Fig. 2c) simulations indicate that part of the Asian temperature response arises from SST anomalies outside the North Atlantic that are associated with the AMO. For example, the north-south gradient in annual-mean temperature response noted above for SST patterns diagnosed from the HadCM3, IPSL, and CSIRO models is weaker when only the North Atlantic part of these SST patterns is used. There is a tendency for the southernmost parts of Asia to cool in those models that simulate cooler north Indian Ocean SST during positive AMO phases, as is evident in the air temperature anomalies above the ocean in Fig. 2b (particularly HadCM3 and CSIRO) that are suppressed in the AMOatl+ experiments (Fig. 2c).

For the AMO- composite, all seven CMIP5 models simulate cold anomalies across the South and East Asia region (Fig. 3a), with a few regional exceptions, and IGCM4 simulates an overall cooling in this region when driven by their SSTA patterns (Fig. 3b), but with additional localized warm anomalies. In the CMIP5 last millennium simulations, the cooling in this region is stronger than the warming during AMO+ phases and Ratna et al. (2019) showed that this can arise from periods with strong volcanic forcing cooling both the North Atlantic and East Asia. Ratna et al. (2019) showed that external forcing (principally the fingerprint of volcanic cooling) changed (strengthened) the correlation between the AMO and Asian climate CMIP5 last millennium simulations. The AMO- SSTA composites used

here to force the IGCM4 may therefore partly represent volcanic cooling effects as well as internal variability, although the volcanic contribution is reduced (see Fig. 4 of Ratna et al. 2019) by using an AMO index with global-mean SST subtracted.

As with the AMO+ composite, the weaker IGCM4 signal when driven by the BCC AMOglo- SSTA pattern might be because that model has the weakest North Atlantic SST anomaly. Similarly, HadCM3 and CSIRO simulate warm anomalies over central and peninsular India during AMO- phases and these characteristics are simulated by IGCM4 when forced by the HadCM3 and CSIRO SSTA patterns (Fig. 3b). However, IGCM4 also simulated warmth in this region for all AMO- SSTA patterns except that diagnosed from CCSM4, and in most cases this warm anomaly is still present when the SSTA is restricted to the North Atlantic (Fig. 3c). This suggests that it may be a dynamical response to cool the North Atlantic SSTA that is present in IGCM4 and in some CMIP5 models.

These results indicate that the intermodel variations arise from differences in each models' AMO-related SST pattern and associated dynamical response to the different SST, which was well simulated by the IGCM4 when forced by the same SSTA patterns (CMIP5). Also, the annual-mean temperature in this region in response to global SSTA and North Atlantic-only SSTA, indicate that part of the Asian temperature response arises from SST anomalies outside the North Atlantic that are associated with the AMO. So, it is important to understand the mechanisms that are responsible for such simulated behavior, which is discussed in the next section.

4. Mechanisms responsible for the AMO influence on South and East Asian climate

This section explores the mechanisms involved in the AMO teleconnection to South and East Asia based on the different SST patterns of the IGCM4 model simulations. First, we consider the midtropospheric circulation response in the AMOglo+ and AMOatl+ experiments, and also for AMOglo- and AMOatl-. We focus this analysis on the summer [May-September (MJJAS)] climate for reasons given earlier.

a. AMOglo+ vs AMOatl+

The AMOglo+ experiment with MEANsst (multimodel-mean SSTA from positive phases of AMO) indicates an extended summer season dynamical response with "positive-negative-positive" 500-hPa geopotential height anomalies over northwestern-central-eastern regions of Asia (Fig. 4a, top panel). This pattern is

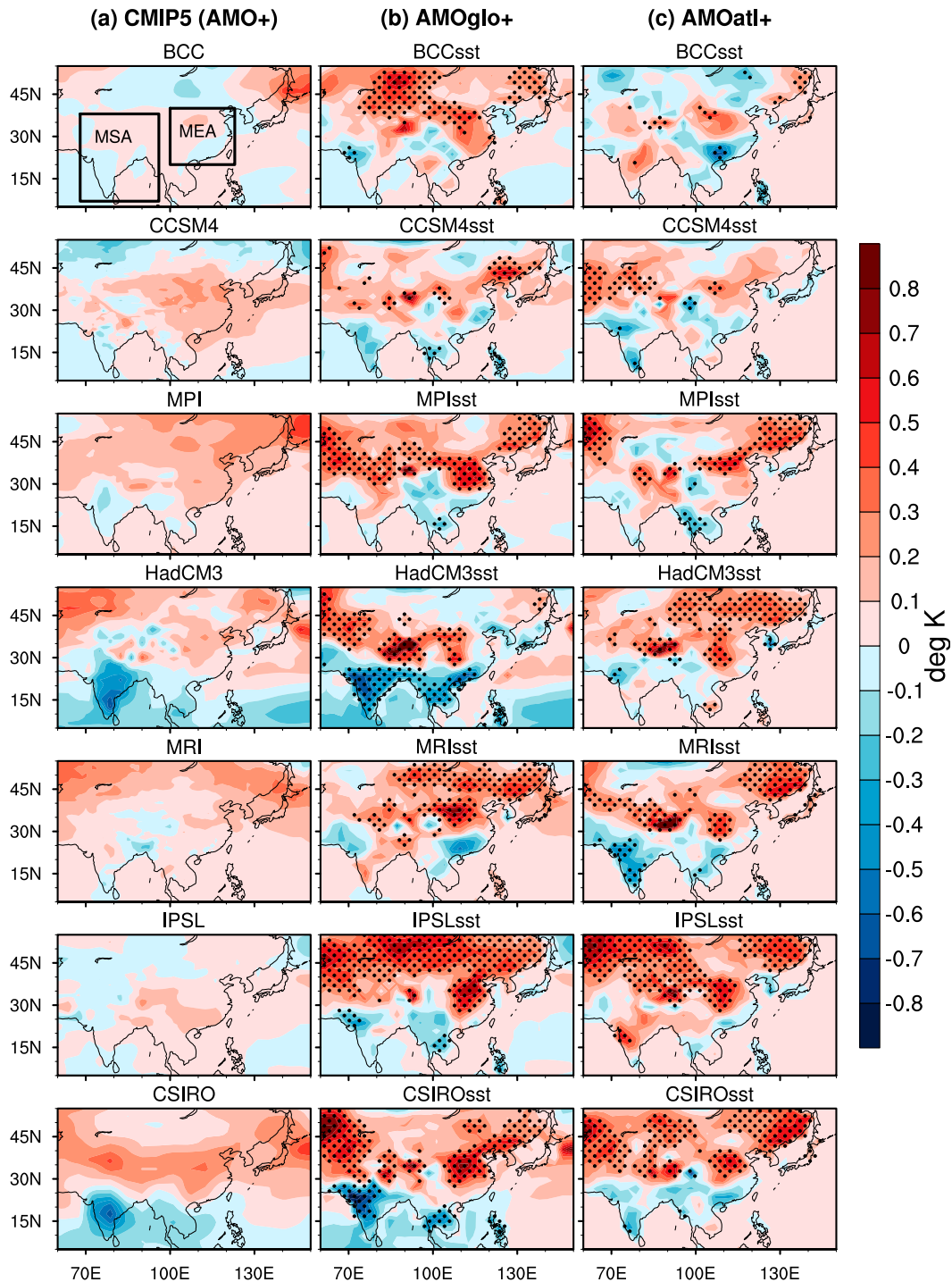


FIG. 2. Surface air temperature anomalies (K) during positive AMO events for (a) CMIP5, (b) IGCM AMOglo+, and (c) IGCM AMOatl+ simulations. Because the IGCM experiments are conducted with $2 \times$ SST anomalies, the CMIP5 values here are multiplied by 2 for comparison. The dotted marks show where the IGCM simulations are significant at 90% level using a Student's t test. The two boxes marked in (a) are the two regions chosen as MSA (5° – 38° N; 68° – 96° E) and MEA (20° – 40° N; 100° – 123° E); for further analysis, see [section 7](#).

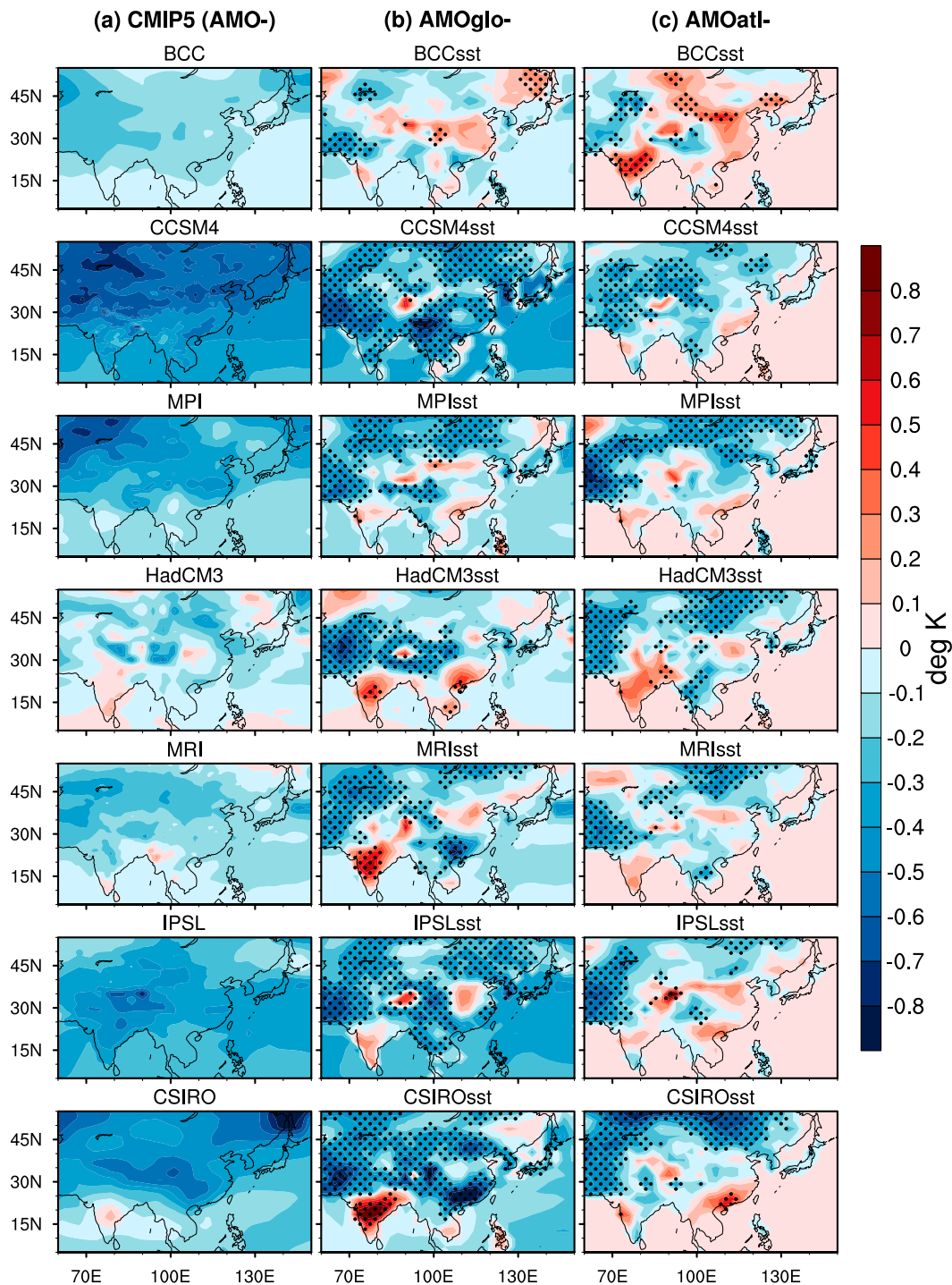


FIG. 3. As in Fig. 2, but for negative AMO events.

part of a Rossby wave train originating over the North Atlantic that is apparent in the 200-hPa meridional wind anomalies and propagates to the Asian region (Fig. S2 in the online supplemental material). Associated with this are “warm–cold–warm” surface temperature

anomalies (Fig. 4b, top panel). The summer anticyclonic circulation simulated at 850 hPa over eastern China/Japan (Fig. 4c, top panel) extends to the upper troposphere indicating the barotropic nature of the circulation. This anticyclonic circulation over the eastern

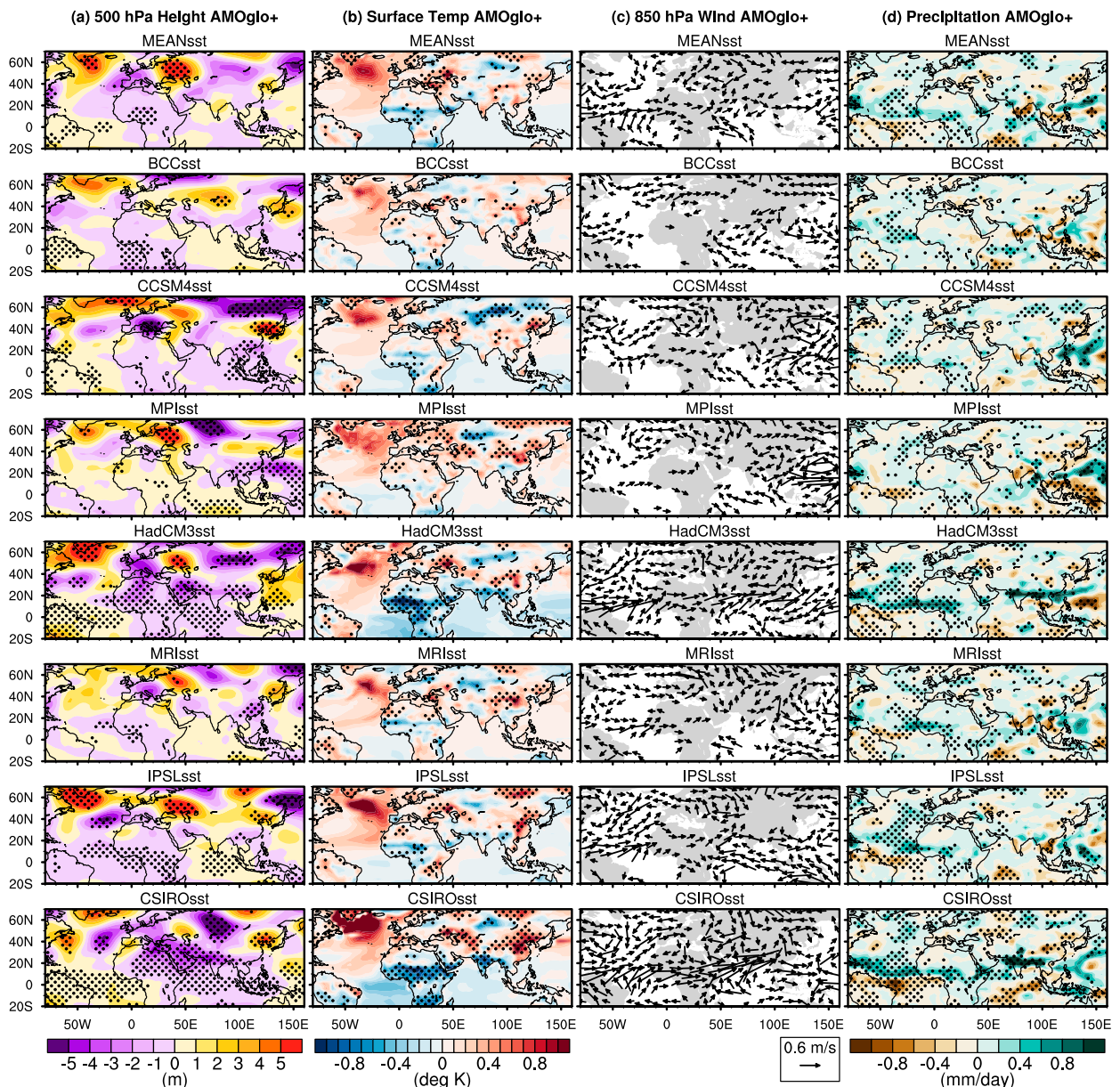


FIG. 4. IGCM-simulated (a) 500-hPa eddy (zonal mean subtracted) geopotential height anomaly (m), (b) surface temperature anomaly (K), (c) 850-hPa wind vector anomaly (m s^{-1}), and (d) precipitation anomaly (mm day^{-1}) for the summer (MJJAS) season for the model experiments conducted with eight different AMOglo+ SSTs anomalies: MEANsst experiments, followed by BCCsst, CCSM4sst, MPIsst, HadCM3sst, MRIsst, IPSLsst, and CSIROsst. The areas with the dotted marks are significant at 90% level using a Student's t test.

China and Japan region reduces precipitation and warms the surface temperature (Figs. 4b,d, top panel).

All seven individual experiments with different SSTA also simulate significantly warm surface temperature anomalies over eastern Asia (Fig. 4b) and the warm anomalies in some of the models are associated with low-level anticyclonic circulation (Fig. 4c) and a barotropic anomalous anticyclone (Fig. 4a). The

position and strength of these features depend on the individual SSTA patterns (e.g., they are stronger with CCSM4sst, MRIsst, and CSIROsst). In experiment BCCsst this anticyclonic circulation anomaly is located over the western Pacific (Fig. 4c) and contributes to a positive precipitation anomaly (Fig. 4d). A strong cyclonic anomaly over the western Pacific with MPIsst (Fig. 4c) weakens the high over China/Japan,

which is seen elongating in the east–west direction (Fig. 4a).

When forced by MEANsst, IGCM4 simulates a positive summer temperature anomaly over the Indian monsoon region (Fig. 4b, top panel), although it is not significant. This coincides with a midtropospheric high pressure anomaly (Fig. 4a, top panel) and a low-level anticyclonic circulation anomaly (Fig. 4c, top panel), leading to reduced precipitation there (Fig. 4d, top panel). With MEANsst, the high is over peninsular India with low to the north (Fig. 4a) but this circulation response and the associated temperature and precipitation anomalies are very sensitive to the AMO+ SSTA pattern. BCCsst, CCSM4sst, MRIsst, and IPSLsst forcing generates this midtropospheric high, whereas HadCM3sst and CSIROsst induce an almost opposite pattern with strong cooling over most of India and strong wetting over northern India (Figs. 4a,b,d). These latter anomalies are caused by strong southwesterly winds flowing toward the Indian landmass (Fig. 4c) that extend up to Southeast Asia where they are also linked with positive precipitation anomalies. In these two simulations (HadCM3sst and CSIROsst), low-level anomalous westerlies extend from the north equatorial Atlantic through north equatorial Africa to the Indian monsoon region, as found during AMO+ events by Krishnamurthy and Krishnamurthy (2016).

Key to initiating this tropical pathway that links the AMO to a response over Asia is a northward shift in the Atlantic ITCZ during the positive phase of the AMO (Zhang and Delworth 2006). We find this northward shift occurs in the IGCM4 simulations (appearing as precipitation dipole in the tropical Atlantic Ocean, Fig. 4d) but we also find that it is sensitive to the AMO+ SSTA patterns. The dipole is particularly clear in the zonal-mean precipitation over the Atlantic domain (Fig. 9a for the ensemble mean). The two simulations (AMOGlo+ HadCM3sst and CSIROsst) with the strongest dipole response (Fig. S3 in the online supplemental material) are those that simulate the strongest westerly circulation and monsoon South Asia precipitation responses. The BCCsst simulation has the weakest ITCZ/dipole response (it lacks the dry anomalies south on the southern edge of the ITCZ; Fig. 4d) likely because some positive SSTA (under AMO+) extend south of the equator in the Atlantic (Fig. 1).

Among the seven different SST patterns, those simulated by HadCM3 (Fig. 1d) and CSIRO (Fig. 1g) show stronger and wider SST anomalies over the tropics, especially over the eastern equatorial Pacific region where they are similar to the La Niña pattern that is conducive for the positive precipitation anomaly over

the Indian region (Sikka 1980; Rasmusson and Carpenter 1982; Ratna et al. 2011; Sikka and Ratna 2011). Applying SSTA only to the North Atlantic (AMOatl+, Fig. 5) removes this response (cooler, wetter Indian summer monsoon) from the HadCM3sst and CSIROsst experiments, and also reduces their ITCZ shift (Fig. S3) so that it is no longer bigger than in the MEANsst experiment. This confirms that the different response to their AMO+ SSTA is driven from outside the North Atlantic. The combined effect of AMO and ENSO on East Asian climate was reported earlier by Dong et al. (2006), Hao and He (2017), and Geng et al. (2017), where they suggested the role of an “atmospheric bridge” to carry the influence of the Atlantic Ocean to the tropical Pacific. Luo et al. (2018) noted that during warm AMO phases, descending motion over the North Pacific may strengthen the extratropical–tropical SST difference, weakening ascent over the tropical Pacific and associated with weaker descending anomalies over the Indian Ocean and higher Indian summer rainfall.

The MEANsst applied only to the North Atlantic (AMOatl+ experiment) shows the wave train more significantly and strongly in terms of its “high–low–high” over the Asian region (Fig. 5a). Again, the midtropospheric high over East Asia associated with the wave train coincides with low-level anticyclonic circulation that causes negative precipitation and warm surface temperature anomalies (Figs. 5b–d). For this experiment there is less sensitivity to the details of the SSTA pattern, though the response strength varies between experiment, with only MRIsst and CSIROsst simulating a response as strongly as the MEANsst case over East Asia.

Comparison of AMOGlo+ (Fig. 4) and AMOatl+ (Fig. 5) simulations indicates that the midlatitude East Asia climate anomalies are forced from the North Atlantic region. SST anomalies outside this region, but still associated with positive AMO phases in the CMIP5 last millennium simulations, strongly influence the climatic response South Asia and in some cases modify the midlatitude response. Since the SST anomalies outside the North Atlantic exhibit more diversity, they contribute most to the diversity of Asian temperature and precipitation anomalies associated with the AMO. All AMOatl+ experiments simulate a northward shift of the Atlantic ITCZ, but the gradient in the precipitation anomaly dipole is weaker when compared with AMOGlo+ in most cases (Fig. 5d and online supplemental Fig. S3), which is clear in the ensemble mean (Fig. 9a).

The results indicate that different SST anomalies associated with AMO+ simulate significantly negative precipitation and warm surface temperature anomalies over

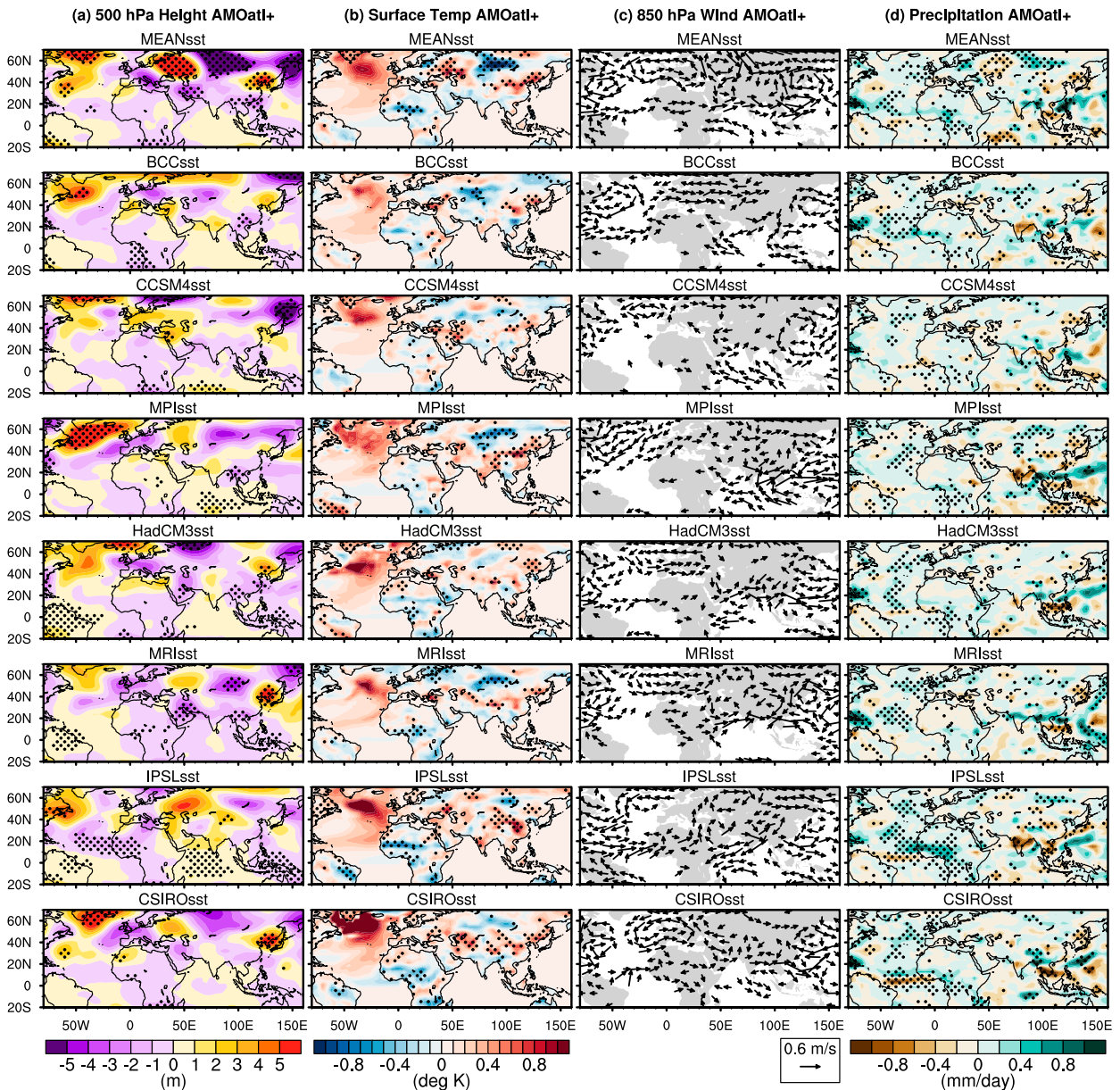


FIG. 5. As in Fig. 4, but for the AMOat+ experiments; i.e., positive AMO SST anomalies are applied only to the North Atlantic and Arctic region.

eastern Asia associated with an anomalous barotropic anticyclone. Similarly, IGCM4 simulates a positive summer temperature and negative precipitation anomaly over the Indian monsoon region, which coincides with a midtropospheric high pressure anomaly and a low-level anticyclonic circulation anomaly. The circulation response and associated temperature and precipitation anomalies over South and East Asia are sensitive to the AMO+ SSTA pattern, especially the patterns outside the North Atlantic. Now, it is interesting to see if the IGCM4 models show similar

behavior for the AMO− anomaly, discussed in the next section.

b. AMO_{glo}− vs AMO_{atl}−

In contrast to the AMO+ response, the midlatitude Rossby wave train is less robust in response to the cool phase of the AMO (online supplemental Fig. S2c). This is especially true for the experiment with SSTA limited to the North Atlantic, which produced a strong wave train for AMOat+ but not for AMOat− over the Asian region (see MEANsst in Figs. S2b,d). The

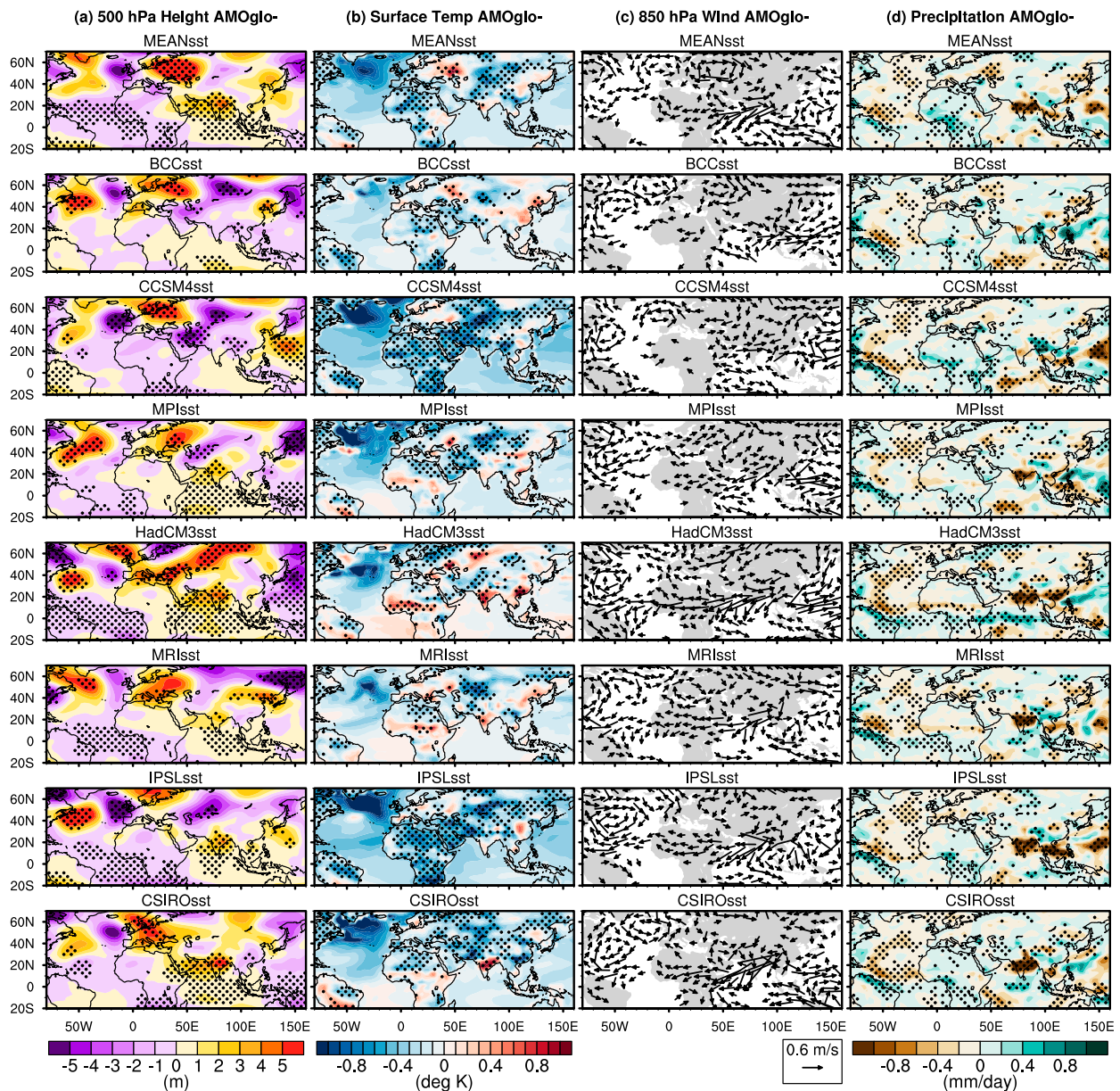


FIG. 6. As in Fig. 4, but for the AMOglo⁻ experiments; i.e., negative AMO SST anomalies are applied globally.

AMO⁻ temperature anomalies over Asia are also less clearly linked to the position of midtropospheric circulation anomalies than they were for AMO⁺, and there are many differences in these anomalies between the different AMOglo⁻ SST cases (Fig. 6a). Instead the cooling over Asia seems to be simply linked to a Northern Hemispheric-wide cooling both over the ocean (Fig. 1) as well as much of the Asian landmass (Fig. 6b). The stronger cooling over land might, therefore, arise partly from the imprint of volcanic cooling on the AMO⁻ SST composite (see section 3). Consequently, the negative temperature anomaly over

East Asia is weaker when the SST forcing is restricted to only the North Atlantic (Fig. 7b cf. Fig. 6b).

A midtropospheric high over India (Fig. 6a) is associated with a northeasterly anomalous low-level wind over the Indian landmass, contributing to dry (Fig. 6d) and warm anomalies (Fig. 6b) over India. These responses to the negative AMO conditions occur in the MEANsst simulation and all of the individual SST simulations except BCCsst and CCSM4sst. This response is weaker but more consistent between simulations when the SST anomalies are only applied to the North Atlantic (Fig. 7; only the MEANsst case does not

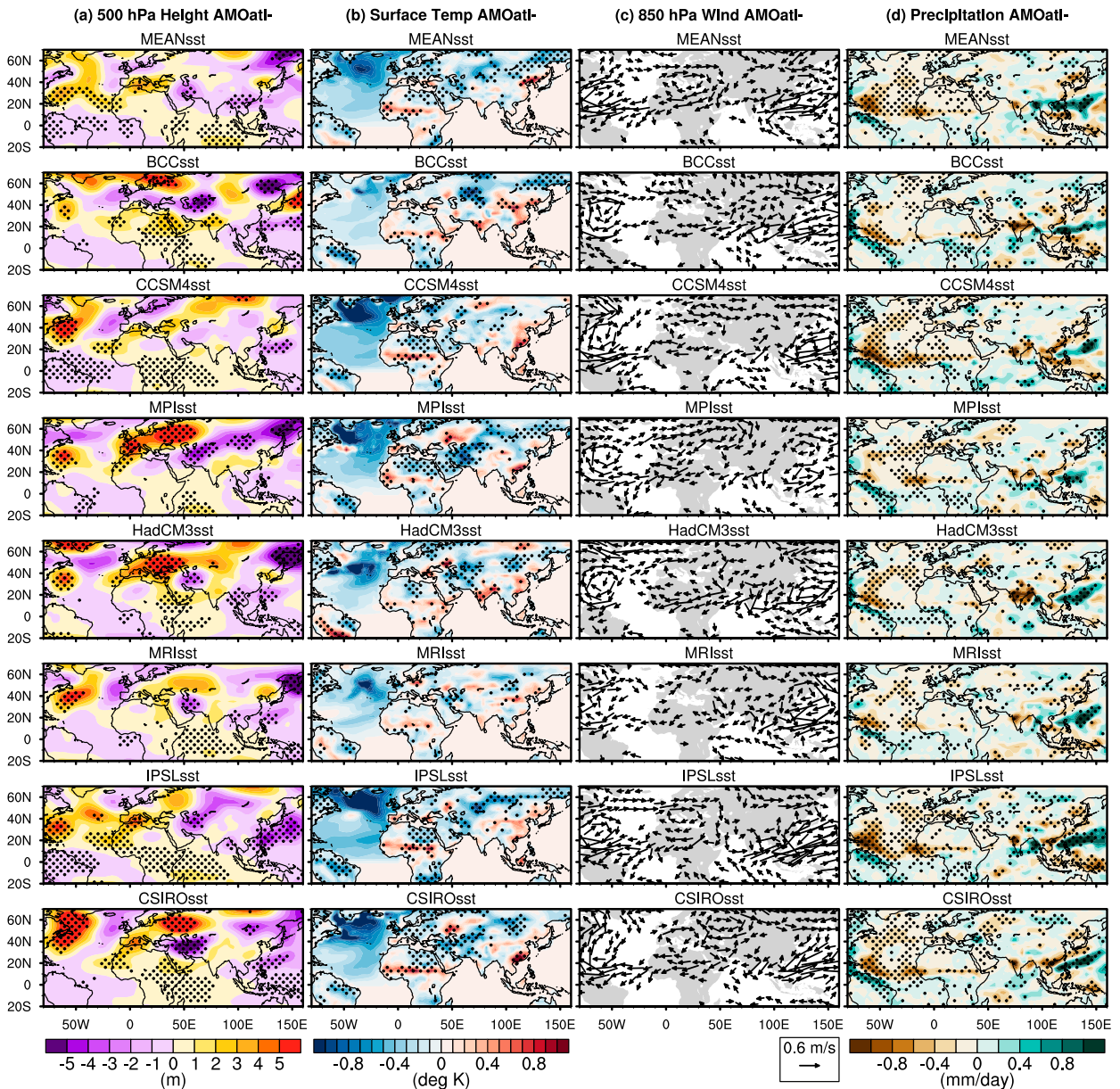


FIG. 7. As in Fig. 4, but for AMOat- experiments; i.e., negative AMO SST anomalies are applied only to the North Atlantic and Arctic region.

show the high pressure and northeasterly flow anomalies over India). This indicates that this AMO teleconnection to a warm and dry Indian summer monsoon arises as a dynamical response to the cool North Atlantic during the negative AMO phase, but it is then modified (sometimes stronger, sometimes weaker) by the SST patterns outside the North Atlantic.

There is a southward shift of the ITCZ and associated precipitation dipole over tropical Atlantic (Figs. 6d, 7d, and 9a), opposite to the AMO+ phase (Figs. 4d, 5d, and 9a). However, the negative precipitation anomaly

(at 12°N) is stronger than the positive anomaly at the equator during the AMO- phase. These changes may be linked with low-level anomalous easterlies extending from South Asian monsoon region to North Africa and further to the tropical Atlantic (Fig. 6c), especially in the AMOglo- experiments (MEANsst, HadCM3sst, MRIsst, IPSLsst, and CSIROsst). They reduce moisture transport to the South Asian region and hence contribute to its negative precipitation anomaly. Only BCCsst and CCSM4sst (AMOGlo-) do not show this anomalous pattern and hence the strength of the negative

precipitation anomaly over South Asia monsoon is much lower than the other AMO_{glo-} experiments.

The ITCZ shift tends to be stronger for AMO_{atl-} than for AMO_{glo-} (Fig. 9a), in contrast to the positive phase forcing when AMO_{glo+} caused a stronger response than AMO_{atl+}. Despite this, the low-level anomalous easterlies and the drying of the South Asian monsoon region are weaker in AMO_{atl-} than in AMO_{glo-}, showing that the tropical pathway linking Atlantic SSTA to the South Asian monsoon is not only dependent on the ITCZ shift and its Atlantic precipitation dipole.

Another common signal in the AMO_{atl-} experiments is the dry anomaly (Fig. 7b) along coastal China accompanied by a coherent wet anomaly (Fig. 7d) in the subtropical western Pacific. This is linked to anomalous cyclonic circulation (Fig. 7c) that causes low-level convergence and contributes to the positive precipitation anomaly over the western Pacific. The associated low-level flow warms the adjacent East Asian landmass by advection (Fig. 7b). This response is disrupted by the different SSTA outside the Atlantic (e.g., the cooler SST in the North Pacific in some AMO₋ composites) and is not consistently seen in the AMO_{glo-} experiments.

The cyclonic circulation over the western Pacific is seen in both AMO_{atl+} (Fig. 5c) and AMO_{atl-} (Fig. 7c), but it is more prominent in AMO_{atl-}. This is the reason we see the significant positive precipitation anomaly over the western Pacific in AMO_{atl-} experiments. Also, there is anomalous northeasterly flow in most of the AMO_{atl-} experiments (Fig. 7c), indicating the weaker monsoon over the Indian region (Fig. 7d). In contrast, we do not see any cyclonic circulation response over the western Pacific in either AMO_{glo+} (Fig. 4c) and AMO_{glo-} (Fig. 6c) experiments. However, an anomalous anticyclonic circulation over the China–Japan region occurs in all AMO_{glo+} experiments except MPIsst (Fig. 4c), associated with the midtropospheric high (Fig. 4a) due to wave train propagating from the North Atlantic.

In summary, the midlatitude Rossby wave train and associated midtropospheric circulation anomalies is less robust in response to the cool phase of the AMO than during the warm phase of the AMO. Also, the cooling over Asia seems to be simply linked to a Northern Hemispheric-wide cooling over both ocean and land, arising partly from the imprint of volcanic cooling on the AMO₋ SST composite. At the same time the results indicate that a warm and dry Indian summer monsoon arises as a dynamical response to the cool North Atlantic during the negative AMO phase. Anomalous easterlies extending from the tropical Atlantic to South Asia

reduce moisture flow to the Indian landmass and hence reduce precipitation.

5. South and East Asian monsoon responses to AMO

Although the response patterns differ between experiments, it is convenient to consider the monsoon precipitation associated with the AMO on an area-averaged basis. We first compare monsoon rainfall (May–September) over South Asia [monsoon South Asia (MSA); 5°–38°N; 68°–96°E] and East Asia [monsoon East Asia (MEA); 20°–40°N; 100°–123°E] with the area-averaged North Atlantic SST (AMO) anomaly (Fig. 8). For MSA, there is a tendency (as shown by the ensemble mean) for increased rainfall with positive AMO and decreased rainfall with negative AMO (Fig. 8a) though the former is only clear for three of eight SST patterns and the latter is only clear for six. There is greater intermodel spread in the strength over the North Atlantic of the AMO₋ SST composites than in the AMO₊ composites, though there is no simple relationship between MSA response and strength of the SST forcing (even when the forcing is restricted to the North Atlantic only; Fig. 8b). Consistent with the earlier analysis of the spatial rainfall patterns, restricting the SST forcing to only the North Atlantic makes the MSA drying more consistent between experiments for the cool AMO phase, and reduces the strongest wetting responses (seen for CSIROsst and HadCM3sst) that were seen for AMO_{glo+}.

The CSIROsst and HadCM3sst forcings in AMO_{glo+} produce the highest wet precipitation anomalies because they induce strong positive vertical wind shear in the north Indian Ocean and over India (Fig. 9c). The vertical wind shear is calculated as the difference between zonal wind at 850 and 200 hPa averaged over 68°–96°E. Variation of vertical wind shear over the Indian subcontinent is associated with the interannual variability of the South Asian monsoon (Webster and Yang 1992; Wang and Fan 1999) and its strong seasonal cycle is used to identify the onset and withdrawal of the Indian summer monsoon (Soman and Kumar 1993; Prasad and Hayashi 2005). CSIROsst and HadCM3sst forcings induce anomalously strong south westerlies over the Arabian Sea and Indian landmass, generating more rainfall over India (Figs. 4c,d). This feature is seen even more clearly in the vertical wind shear positive anomaly (Fig. 9c), as is the suppression of this signal when SST forcing is restricted to the North Atlantic (Fig. 9d). In the latter case (AMO_{atl+}), strong vertical wind shear negative anomalies are caused by the MPIsst and IPSLsst forcings (Fig. 9d) and

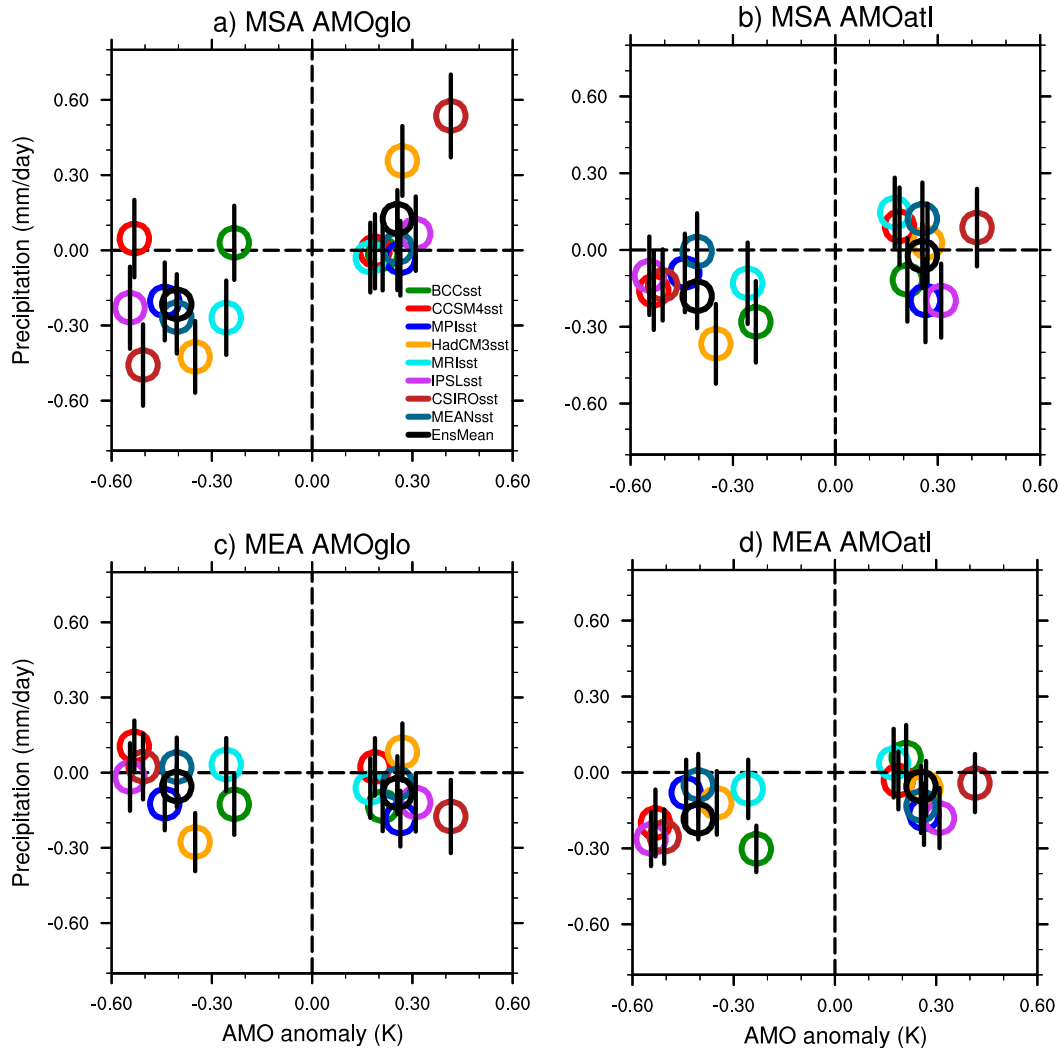


FIG. 8. AMO SST anomalies (K) and corresponding IGCM-simulated summer (MJJAS) area-averaged (a),(b) monsoon South Asia precipitation (5° – 38° N; 68° – 96° E) and (c),(d) monsoon East Asia precipitation (20° – 40° N; 100° – 123° E) anomaly for each experiment with AMO+ and AMO– SST anomalies for (left) AMOGlo and (right) AMOatl experiments. The mean response from seven IGCM experiments is also shown as EnsMean for comparison with the MEANsst experiment (where the mean of the seven SST patterns was used to force the IGCM). The vertical lines show the standard errors of the respective model experiments.

associated with drier conditions over the Indian region (Fig. 8b).

In the case of the AMOGlo– experiments, there is also correspondence between the MSA precipitation anomalies (Fig. 8a) and the vertical wind shear anomalies (Fig. 9e): positive shear anomalies are generated in the two cases (BCCsst and CCSM4sst) with wetter MSA, and negative shear anomalies in five cases with drier MSA. Only for IPSLsst was there near-zero wind shear anomalies but a significant reduction in MSA precipitation. The tropical wind shear anomalies are much reduced when the SST forcing is restricted to the North Atlantic (Fig. 9f), indicating that the remaining dry

MSA anomalies (Fig. 8b) arise from other mechanisms discussed in section 4.

The zonal-mean precipitation anomaly over the Atlantic domain (Fig. 9a) shows that AMOGlo+ causes a northward shift of the ITCZ. This shift is strongest for the HadCM3 and CSIRO SST patterns (online supplemental Fig. S3) and these are the two cases with the strongest AMOGlo+ precipitation response over monsoon South Asia (Fig. 8a). The ensemble mean shows the peak of the positive component of dipole along 11° N and the peak negative component along 2° N, with a sharp gradient between. A northward shift of the Atlantic ITCZ is also caused by AMOatl+ SSTA, but there is weaker gradient

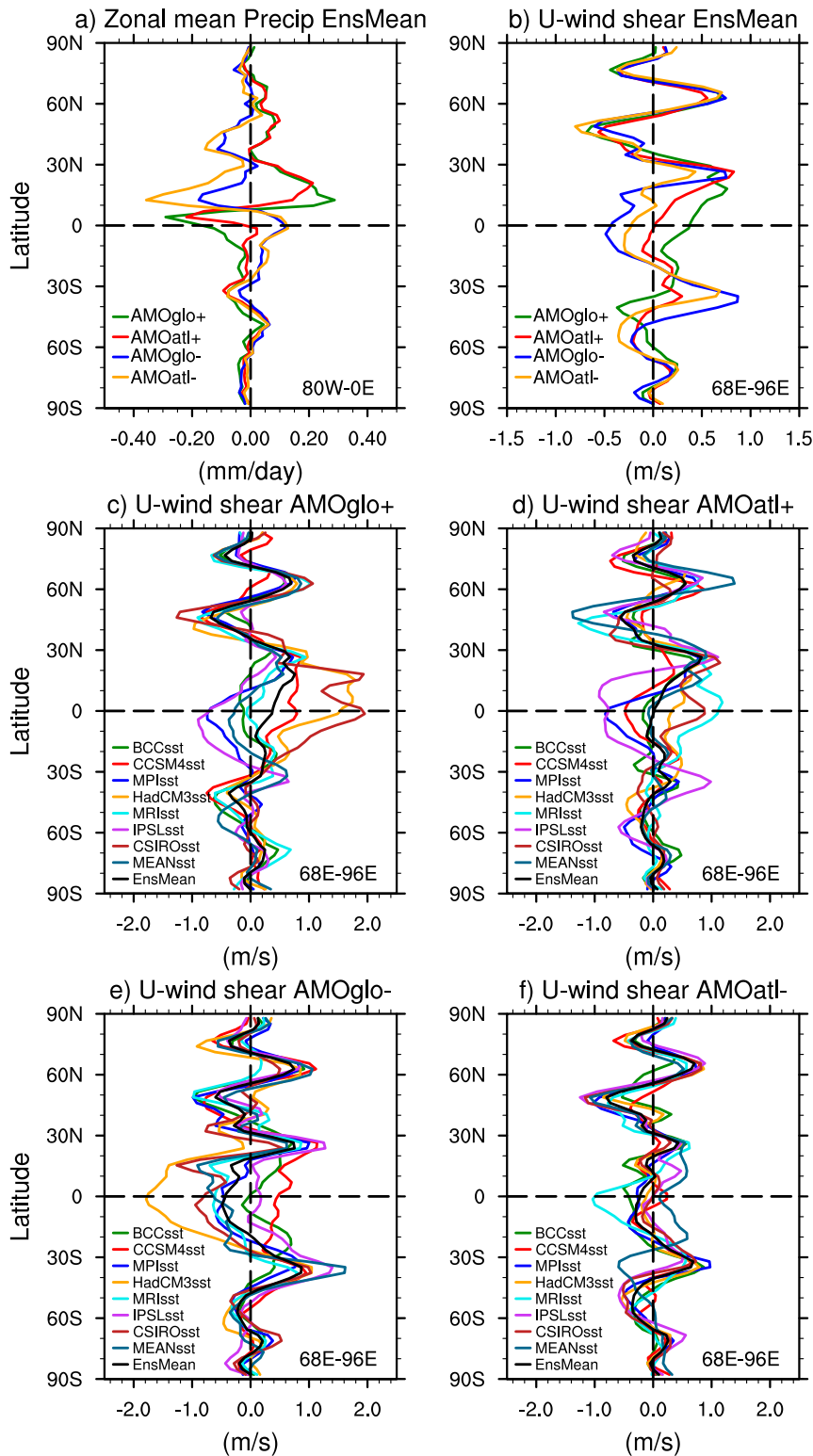


FIG. 9. (a) IGC4-simulated summer (MJAS) zonal-mean precipitation anomaly (mm day^{-1}) over the Atlantic region ($80^{\circ}\text{W}-0^{\circ}$) for the ensemble mean of seven runs for each AMOglo+, AMOatl+, AMOglo-, and AMOatl- experiment; (b) as in (a), but for vertical zonal wind shear ($850 - 200$ hPa) averaged over the South Asian monsoon region ($68^{\circ}-96^{\circ}\text{E}$); and as in (b), but for eight different SST forcings for (c) AMOglo+, (d) AMOatl+, (e) AMOglo-, and (f) AMOatl- experiments.

in the precipitation dipole. With the negative phase of the AMO, we see a dipole precipitation anomaly with opposite sign indicating a southward shift of the Atlantic ITCZ, and in contrast to AMO+ forcing, the gradient is now sharper when SSTA forcing is limited to the North Atlantic compared to when it is applied globally (AMOatl− and AMOglo− in Fig. 9a). For individual AMOglo− SSTA patterns there is a partial association between the Atlantic ITCZ shift (Fig. S3) and precipitation response over monsoon South Asia (Fig. 8a): the three experiments with the biggest Atlantic precipitation reduction at 11°N (MRIss, HadCM3sst, CSIROsst) are also the three with the largest reduction in MSA precipitation (they also show strong reductions in wind shear over the Indian Ocean region (Fig. 9e). This relationship, however, does not hold up when the SSTA is applied only to the North Atlantic.

Most experiments, whether with AMOglo or AMOatl and whether for cool or warm phases of the AMO, simulate weak negative precipitation anomalies over the MEA region (Figs. 8c,d). The weak responses are consistent with the analysis of response patterns (section 4), which showed spatial variation in the MEA region rather than coherent anomalies. The negative anomalies for both AMOatl− and AMOatl+ forcings indicates a possibly nonlinear response. The earlier analysis suggests that a more coherent response in East Asia may be found for temperature rather than precipitation.

In summary, the area-averaged SST anomaly indicates that there is greater intermodel spread in the strength over the North Atlantic of the AMO− SSTA composites than in the AMO+ composites, though there is no simple relationship between MSA response and strength of the SST forcing. However, restricting the SST forcing to only the North Atlantic makes the MSA drying more consistent between experiments for the cool AMO phase. The positive (negative) precipitation anomaly during AMO+ (AMO−) is associated with a northward (southward) shift of the Atlantic ITCZ (Fig. 9a) and strong positive (negative) vertical wind shear anomaly (Fig. 9b) over the Indian subcontinent, supporting a tropical pathway linking the AMO with monsoon South Asia.

The above results indicated that the simulated precipitation and temperature of the South and East Asia are related to the SST patterns over North Atlantic associated with AMO. The different SST anomalies obtained from CMIP5 simulations also show different AMO intensity apart from its spatial patterns. In the next section we analyze the intensity of the simulated temperature and precipitation related

to the intensity of the positive and negative phases of AMO.

6. Nonlinearity of response to AMO anomaly amplitude

We found that IGCM4-simulated similar annual-mean temperature anomalies over South and East Asia as found in the CMIP5 last millennium simulations (Figs. 2 and 3). It is interesting to see if the intensity of the simulated temperature anomalies is related to the amplitude of the AMO anomalies (both for AMO+ and AMO− events). To investigate this we have calculated the area-averaged temperature for the same region analyzed by Ratna et al. (2019)—land grid cells averaged over the region 5°–55°N and 60°–150°E—and compared against the area-averaged North Atlantic (0°–65°N, 80°W–0°) SSTA. We considered annual means for comparison with Ratna et al. (2019), extended summer means as the main focus of this paper, and extended winter means as they show contrasting behavior to the summer. We analyzed linearity with two approaches. First, the existing experiments (forced by 2×SST for each case) already provide a range of forcing strengths because each composite has a different mean SSTA over the North Atlantic (especially for the negative AMO phases) and linearity between positive and negative phases can also be considered. However, the SST patterns are different among the eight sets of experiments and between the AMO+ and AMO− phases (which are not simply the opposite sign) so it is difficult judge whether the nonlinearity is due to the SSTA amplitude or pattern. The second approach uses the same SST patterns (the multimodel means, i.e., MEANsst over the North Atlantic only) and scaled with a magnitude between 1 and 5 times (hereinafter 1×SST–5×SST) for both positive and negative phases of AMO.

We find a positive relationship between the surface temperature anomaly in this larger SEA region and the mean North Atlantic SST anomaly (Fig. 10). The annual-mean SEA temperature anomaly is approximately proportional to the annual-mean North Atlantic SST anomaly (Fig. 10a), with the larger responses to AMO− mostly reflecting that the SSTA composites are more intense for AMO− than for AMO+ (Fig. 1). The relationship is more nonlinear for the extended summer (Fig. 10c) due to a strong SEA cooling with AMO− but only a weak response to AMO+. Conversely, the average response to AMO+ is stronger than to AMO− in the extended winter (Fig. 10e). When the SST forcing is applied only to the North Atlantic (AMOatl), the AMO− responses tend to weaken (especially for the annual and summer means, Figs. 10b,d) but the response to AMO+ forcing is not consistently changed. So, we

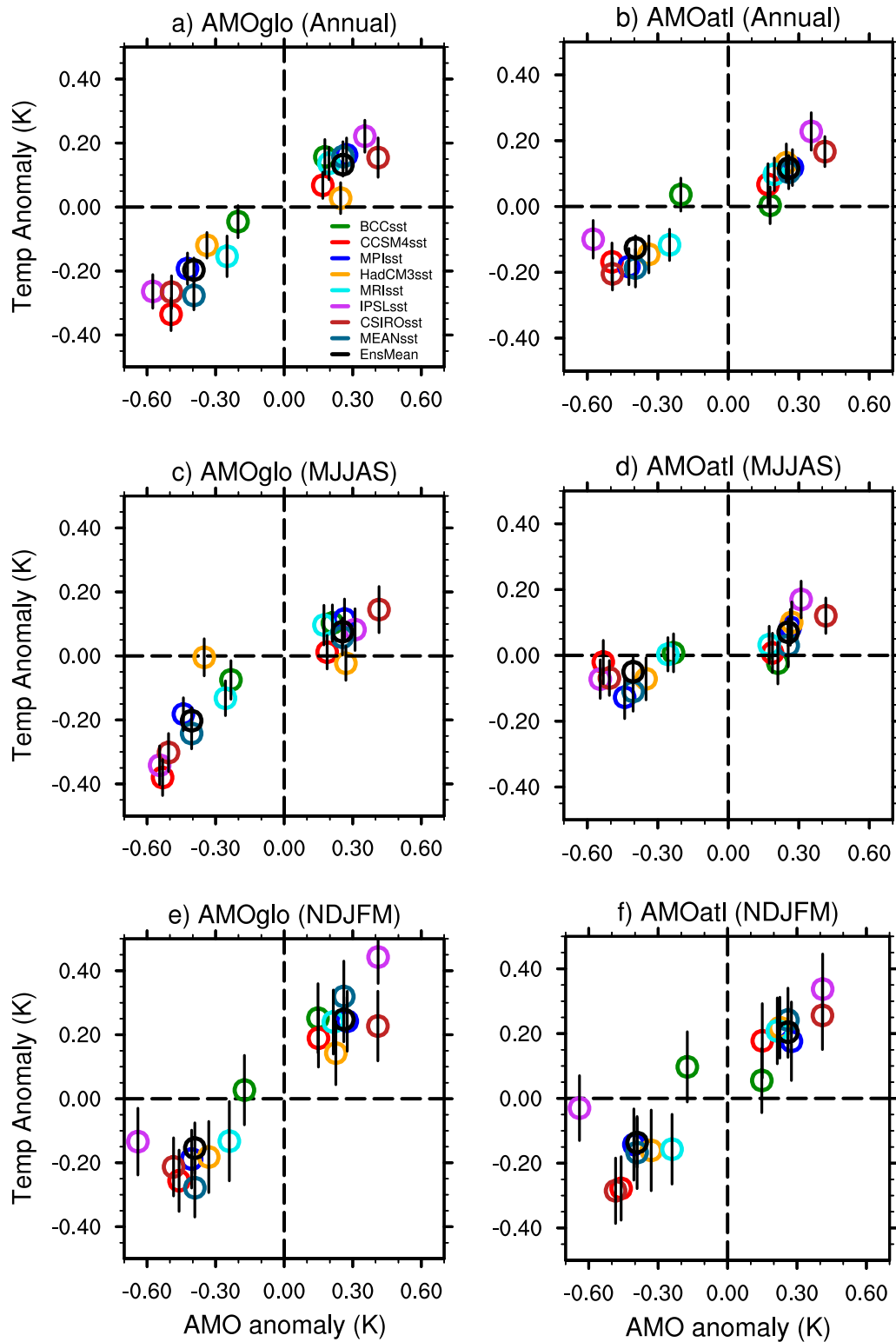


FIG. 10. AMO SST anomalies (K) and corresponding IGCM-simulated area-averaged South and East Asian surface temperature (5° – 55° N; 60° – 150° E) anomaly for each experiments with AMO+ and AMO– SST anomalies for (left) AMOGlo and (right) AMOatl for (a),(b) annual, (c),(d) MJJAS, and (e),(f) November–March means. The mean response from seven IGCM experiments is also shown as EnsMean for comparison with the MEANsst experiment (where the mean of the seven SST patterns was used to force the IGCM). The vertical bars show the standard errors of the respective model experiments.

conclude that the overall response to the AMO SST forcing is somewhat nonlinear because the summer response to negative phase AMO forcing is enhanced by the concomitant SST anomalies outside the North Atlantic.

For individual models, we see more complex behavior. BCCsst has a weaker response than the other experiments (Figs. 10a,b) for AMOatl+, AMOatl− and AMOglo−, and even shows slight warming over SEA for some AMO− cases. The IPSLsst and CSIROsst have strong AMO− and AMO+ mean Atlantic SSTA and produce some of the strongest SEA surface temperature anomalies, but with a few notable exceptions (e.g., the winter North Atlantic AMO− forcing is strongest for IPSLsst but when this pattern is applied only to the North Atlantic, there is no significant cooling over SEA; Fig. 10f). The Atlantic SST negative anomaly for CCSM4sst is among the strongest for AMO− (and weakest for AMO+) and it also has among the coldest SEA surface temperature anomaly *except* in summer when the AMO forcing is only applied to the North Atlantic (AMOatl−; Fig. 10d). In that experiment, there is no significant cooling over SEA, so the very strong summer cooling in CCSM4glo− must be forced by the extensive negative SST anomalies outside the North Atlantic that are associated with negative AMO phases in CCSM4 (Fig. 1). In contrast, the AMO+ response seems to only come from the North Atlantic as both AMOglo+ and AMOatl+ show similar responses.

For the experiments in which we scaled the strength of the fixed pattern (MEANsst, over the North Atlantic only) of SST anomalies, we analyzed the area-averaged response of both temperature and precipitation, considering their annual means over land grid cells in the SEA region, as well as for the overall NH and SH landmasses (Fig. 11). Over the SEA region (Figs. 11a,b), temperature has a linear response to North Atlantic SST anomaly associated with both AMO+ and AMO−, but the precipitation response is nonlinear between AMO− and AMO+. The temperature response during AMO− is stronger than during AMO+, but so is the SST anomaly in the North Atlantic (Figs. 1h,q). Precipitation, over SEA tends to decrease in proportion to the AMO− forcing strength, but there is no clear increase (and sometimes a negative precipitation anomaly) associated with warm AMO+ anomalies.

The NH land response is similar to the SEA region: approximate linearity of surface temperature response across both AMO− and AMO+, linearity of precipitation response to AMO− but nonlinear for the weak response to AMO+ forcing and across both AMO− and AMO+ phases. The SH land surface cools during both AMO+ and AMO− phase and thus do not show linearity across both the phases. This is surprising and suggests a nonlinear dynamical response rather than simple

thermal cooling (the SSTA in these experiments are applied only to the North Atlantic, so the hemispheric seesaw in SST associated with the AMO shown in Fig. 1 is not the cause of this response). The response of SH land precipitation is very weak, showing little change for AMO+ phase forcing and a weak increase as negative SST anomalies strengthen during AMO− phase forcing. For much stronger high-latitude heating and in a more idealized model, we found a strong nonlinear response of precipitation over South and East Asia and analyzed the mechanisms that generated the response (Talento et al. 2020).

7. Conclusions

In this study we explored the relation between summer climate over South and East Asia and its dependence on the SST patterns associated with positive and negative phases of AMO. We examined the temperature and precipitation responses in the SEA region to AMO-like SST anomalies, globally as well as in the North Atlantic Ocean only, using sets of idealized model experiments with IGCM4. The main conclusions obtained in this study are given below.

- (i) IGCM4 produces surface temperature anomalies over the SEA region that are similar to those simulated by CMIP5 models. The surface temperature for the overall SEA region shows positive (negative) anomalies during the warm (cold) phase of AMO in both the CMIP5 composites and SST-forced IGCM4 simulations. The intermodel variations arise partly from differences in each models' AMO-related SST pattern and partly from each model's dynamical response to the different SST. IGCM4 simulations indicate that part of the Asian temperature response arises from SST anomalies outside the North Atlantic that are associated with the AMO.
- (ii) Our results indicate that the AMO influences the summer climate of East Asia through an extratropical atmospheric circulation pathway. A Rossby wave train originates in the North Atlantic during the warm phase of AMO and propagates eastward (online supplemental Figs. S2a,b), leading to a potential connection between the North Atlantic SST and the Asian climate (evident in the 500-hPa geopotential height, Figs. 4 and 5). The wave train is more robust when IGCM4 is forced by the SST anomaly only in the North Atlantic rather than by using the global SST anomaly associated with the warm phase of AMO. Different SST anomalies associated with AMO+ simulate significantly negative precipitation and warm surface temperature anomalies over eastern Asia associated with an anomalous barotropic anticyclone.

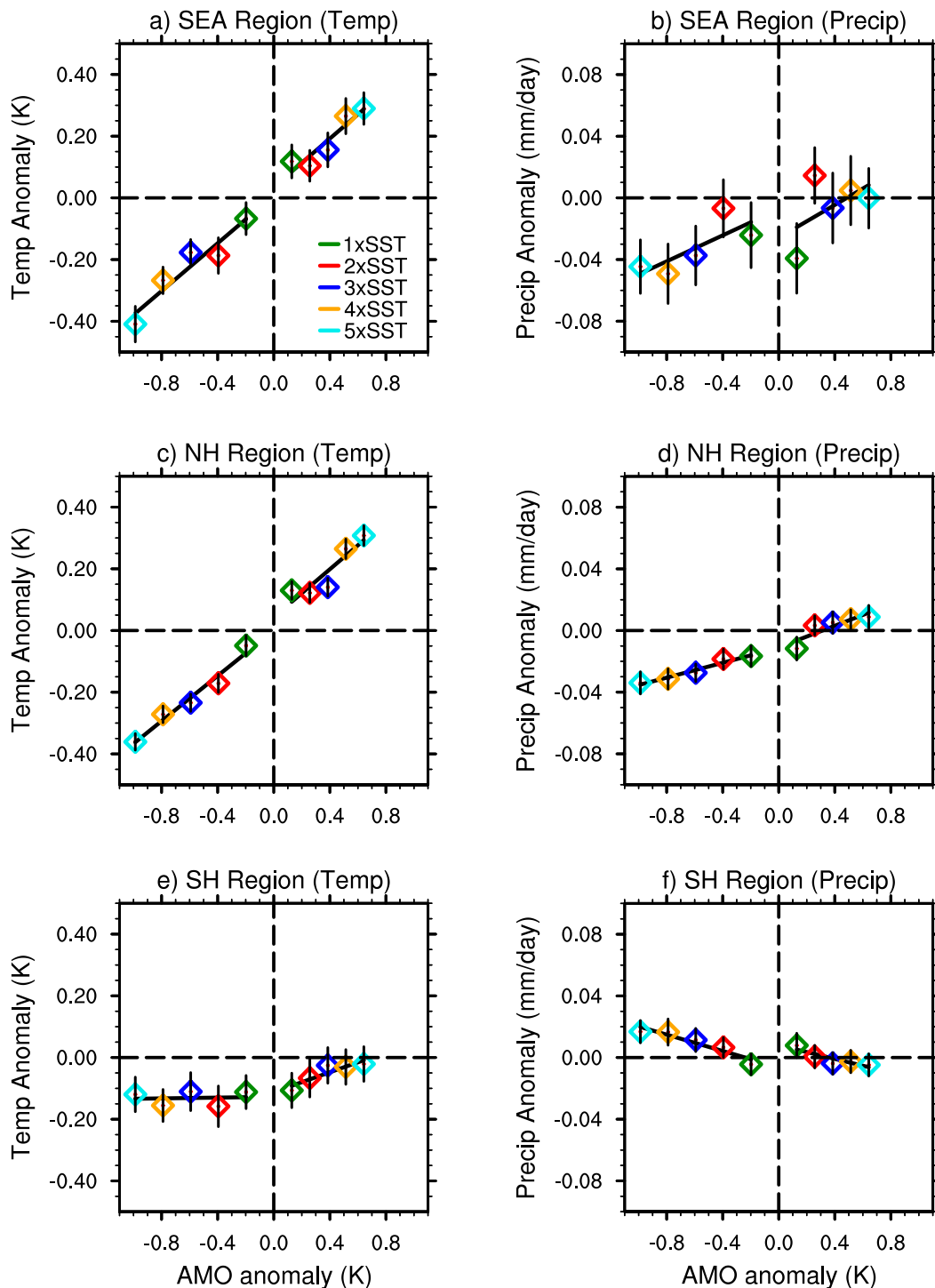


FIG. 11. Nonlinearity of (left) temperature and (right) precipitation response to 1–5 times the AMO SST anomaly (applied to the North Atlantic only; 1×SST–5×SST) for both positive and negative phases of AMO; the area-averaged temperature and precipitation is calculated over the land grid points only for the (a),(b) SEA region, (c),(d) Northern Hemisphere, and (e),(f) Southern Hemisphere. The vertical bars show the standard errors of the respective model experiments. The solid black line is the linear least squares fit calculated separately for AMO+ and AMO– anomalies.

- (iii) The midlatitude Rossby wave train and associated midtropospheric circulation anomalies is less robust in response to the cool phase of the AMO. Cooling over Asia seems to be simply linked to a NH-wide cooling both over the ocean and land. The widespread SST cooling of the AMO[−] patterns (Fig. 1) arises partly from the imprint of volcanic cooling during the simulations from which these patterns were diagnosed (Ratna et al. 2019).
- (iv) The precipitation over South Asia is linked to the AMO partly via a tropical pathway. In response to AMO[−] SST patterns, IGCM4 simulates a southward shift of the Atlantic ITCZ linked to low-level anomalous easterlies extend across North Africa and into the South Asian monsoon. This reduces the moisture transport to South Asia, which, alongside a reduction in vertical wind shear in the Indian Ocean region, leads to drying of the South Asian monsoon. This mechanism is less clear for the positive AMO phase: although there is a northward shift of the Atlantic ITCZ, it is only for the two SST patterns where this shift is strongest that it is linked, via anomalous westerlies extending from tropical Atlantic to South Asian landmass, to enhanced rainfall over India. This behavior disappears when limiting the AMO⁺ SST patterns to only the North Atlantic.

These tropical and extratropical pathways that cause a response of the South and East Asia summer climate to the AMO are sensitive, therefore, to the pattern of AMO SST anomalies, and to whether they are confined to the North Atlantic and Arctic or are more widespread.

- (v) Over the overall SEA region, temperature has a linear response to the strength and sign of the AMO North Atlantic SST anomaly, but the precipitation response is nonlinear—particularly when comparing across the negative and positive phases of the AMO. The temperature response during AMO[−] is stronger than during AMO⁺, with the larger responses to AMO[−] mostly reflecting that the SSTA composites are more intense for AMO[−] than for AMO⁺. IGCM4 simulates a decrease in precipitation over SEA for AMO[−], which tends to strengthen as the SST forcing increases from 2xSST to 5xSST, but there is no clear increase (and sometimes a negative precipitation anomaly) associated with warm AMO⁺ anomalies.

The different teleconnections between AMO and Asian climate in the PMIP/CMIP5 simulations can arise from a combination of different AMO SST patterns and different AGCM behaviors in those coupled models. By designing a set of experiments with the same AGCM

(the IGCM4) but different AMO SST patterns, we are able to explore one aspect (AMO-related SST pattern) while controlling for the other (AGCM dependence). But our results themselves may be dependent on the particular model used here (IGCM4) because the atmospheric response to the same SSTA is model dependent (e.g., Schubert et al. 2009; Lin et al. 2016). We partly assessed this model dependence by the comparison of IGCM4's surface temperature response over our study region how the IGCM's response with the original PMIP/CMIP5 responses to their AMO patterns (Figs. 2 and 3).

The results obtained in this study help in understanding further the potential for the AMO to generate multi-decadal variability in South and East Asian climate. Ratna et al. (2019) already showed that the presence of external forcing can affect the empirical relationship between the internal variability of the AMO and East Asian climate and that this relationship shows considerable spread between climate models. Here, we show that part of this model diversity arises because each climate model simulates an AMO with a different pattern of SST anomalies and this can affect the atmospheric response to the SST forcing. This is particularly the case for SST anomalies outside the North Atlantic that are nevertheless associated with AMO variability and can alter the climate over the South Asian region.

Acknowledgments. This study is supported by the Belmont Forum and JPI-Climate project INTEGRATE (An Integrated Data-Model Study of Interactions between Tropical Monsoons and Extratropical Climate Variability and Extremes) with funding by U.K. NERC Grant NE/P006809/1. The model experiments were conducted on the High Performance Compute Cluster at the University of East Anglia. The authors thank three anonymous reviewers for their constructive comments.

Data Availability Statement. The composite mean AMO SST patterns and the model-simulated data used for this manuscript are available at the Centre for Environmental Data Analysis (CEDA) archive at <http://dx.doi.org/10.5285/3f2f92ad04f84e65a2399deafdf8bbbc>.

REFERENCES

- An, Z. S., and Coauthors, 2015: Global monsoon dynamics and climate change. *Annu. Rev. Earth Planet. Sci.*, **43**, 29–77, <https://doi.org/10.1146/annurev-earth-060313-054623>.
- Booth, B. B. B., N. J. Dunstone, P. R. Halloran, T. Andrews, and N. Bellouin, 2012: Aerosols implicated as a prime driver of twentieth-century North Atlantic climate variability. *Nature*, **484**, 228–232, <https://doi.org/10.1038/nature10946>.
- Chylek, P., C. K. Folland, H. A. Dijkstra, G. Lesins, and M. K. Dubey, 2011: Ice-core data evidence for a prominent near 20 year time-scale of the Atlantic multidecadal oscillation. *Geophys. Res. Lett.*, **38**, L13704, <https://doi.org/10.1029/2011GL047501>.

- Coats, S., and J. E. Smerdon, 2017: The Atlantic's internal drum beat. *Nat. Geosci.*, **10**, 470–471, <https://doi.org/10.1038/ngeo2970>.
- Compo, G. P., and Coauthors, 2011: The Twentieth Century Reanalysis Project. *Quart. J. Roy. Meteor. Soc.*, **137**, 1–28, <https://doi.org/10.1002/qj.776>.
- Cubasch, U., R. Voss, G. C. Hegerl, J. Waszkewitz, and T. J. Crowley, 1997: Simulation of the influence of solar radiation variations on the global climate with an ocean–atmosphere general circulation model. *Climate Dyn.*, **13**, 757–767, <https://doi.org/10.1007/s003820050196>.
- Delworth, T. L., and M. E. Mann, 2000: Observed and simulated multidecadal variability in the Northern Hemisphere. *Climate Dyn.*, **16**, 661–676, <https://doi.org/10.1007/s003820000075>.
- , S. Manabe, and R. J. Stouffer, 1993: Interdecadal oscillation of the thermohaline circulation in a coupled ocean–atmosphere model. *J. Climate*, **6**, 1993–2011, [https://doi.org/10.1175/1520-0442\(1993\)006<1993:IVOTTC>2.0.CO;2](https://doi.org/10.1175/1520-0442(1993)006<1993:IVOTTC>2.0.CO;2).
- Ding, Q., and B. Wang, 2005: Circumglobal teleconnection in the Northern Hemisphere summer. *J. Climate*, **18**, 3483–3505, <https://doi.org/10.1175/JCLI3473.1>.
- Dong, B. W., R. T. Sutton, and A. A. Scaife, 2006: Multidecadal modulation of El Niño–Southern Oscillation (ENSO) variance by Atlantic Ocean sea surface temperatures. *Geophys. Res. Lett.*, **33**, L08705, <https://doi.org/10.1029/2006GL025766>.
- Enfield, D. B., A. M. Mestasnunez, and P. Trimble, 2001: The Atlantic multi-decadal oscillation and its relation to rainfall and river flows in the continental US. *Geophys. Res. Lett.*, **28**, 2077–2080, <https://doi.org/10.1029/2000GL012745>.
- Fang, K., and Coauthors, 2019: Interdecadal modulation of the Atlantic Multi-decadal Oscillation (AMO) on southwest China's temperature over the past 250 years. *Climate Dyn.*, **52**, 2055–2065, <https://doi.org/10.1007/s00382-018-4244-x>.
- Feng, S., and Q. Hu, 2008: How the North Atlantic multidecadal oscillation may have influenced the Indian summer monsoon during the past two millennia. *Geophys. Res. Lett.*, **35**, L01707, <https://doi.org/10.1029/2007GL032484>.
- , O. Hu, and R. J. Oglesby, 2011: Influence of Atlantic sea surface temperatures on persistent drought in North America. *Climate Dyn.*, **37**, 569–586, <https://doi.org/10.1007/s00382-010-0835-x>.
- Fleitmann, D., S. J. Burns, M. Mudelsee, U. Neff, J. Kramers, A. Mangini, and A. Matter, 2003: Holocene forcing of the Indian monsoon recorded in a stalagmite from southern Oman. *Science*, **300**, 1737–1739, <https://doi.org/10.1126/science.1083130>.
- Folland, C. K., T. N. Palmer, and D. E. Parker, 1986: Sahel rainfall and worldwide sea temperatures, 1901–85. *Nature*, **320**, 602–607, <https://doi.org/10.1038/320602a0>.
- Forster, P. M. de F., M. Blackburn, R. Glover, and K. P. Shine, 2000: An examination of climate sensitivity for idealized climate change experiments in an intermediate general circulation model. *Climate Dyn.*, **16**, 833–849, <https://doi.org/10.1007/s003820000083>.
- Gao, L. H., Z. W. Yan, and X. W. Quan, 2014: Observed and SST-forced multi-decadal variability in global land surface air temperature. *Climate Dyn.*, **44**, 359–369, <https://doi.org/10.1007/s00382-014-2121-9>.
- Geng, X., W. Zhang, M. F. Stuecker, P. Liu, F. Jin, and G. Tan, 2017: Decadal modulation of the ENSO–East Asian winter monsoon relationship by the Atlantic multidecadal oscillation. *Climate Dyn.*, **49**, 2531–2544, <https://doi.org/10.1007/s00382-016-3465-0>.
- Ghosh, R., W. A. Müller, J. Baehr, and J. Bader, 2016: Impact of observed North Atlantic multidecadal variations to European summer climate: A linear baroclinic response to surface heating. *Climate Dyn.*, **48**, 3547–3563, <https://doi.org/10.1007/s00382-016-3283-4>.
- Goldenberg, S. B., C. W. Landsea, A. M. Mestas-Nuñez, and W. M. Gray, 2001: The recent increase in Atlantic hurricane activity: Causes and implications. *Science*, **293**, 474–479, <https://doi.org/10.1126/science.1060040>.
- Goswami, B. N., M. S. Madhusoodanan, C. P. Neema, and D. Segupta, 2006: A physical mechanism for North Atlantic SST influence on the Indian summer monsoon. *Geophys. Res. Lett.*, **33**, L02706, <https://doi.org/10.1029/2005GL024803>.
- Gray, W. M., J. D. Sheaffer, and C. W. Landsea, 1997: Climate trends associated with multidecadal variability of Atlantic hurricane activity. *Hurricanes: Climate and Socioeconomic Impacts*, H. F. Diaz and R. S. Pulwarty, Eds., Springer, 15–53.
- Greatbatch, R. J., X. Sun, and X.-Q. Yang, 2013: Impact of variability in the Indian summer monsoon on the East Asian summer monsoon. *Atmos. Sci. Lett.*, **14**, 14–19, <https://doi.org/10.1002/asl2.408>.
- Grossmann, I., and P. J. Klotzbach, 2009: A review of North Atlantic modes of natural variability and their driving mechanisms. *J. Geophys. Res.*, **114**, D24107, <https://doi.org/10.1029/2009JD012728>.
- Gupta, A. K., D. M. Anderson, and J. T. Overpeck, 2003: Abrupt changes in the Asian southwest monsoon during the Holocene and their links to the North Atlantic Ocean. *Nature*, **421**, 354–357, <https://doi.org/10.1038/nature01340>.
- Hao, X., and S. He, 2017: Combined effect of ENSO-like and Atlantic multidecadal oscillation SSTAs on the interannual variability of the East Asian winter monsoon. *J. Climate*, **30**, 2697–2716, <https://doi.org/10.1175/JCLI-D-16-0118.1>.
- Hoskins, B. J., and M. J. Rodwell, 1995: A model of the Asian summer monsoon. Part I: The global scale. *J. Atmos. Sci.*, **52**, 1329–1340, [https://doi.org/10.1175/1520-0469\(1995\)052<1329:AMOTAS>2.0.CO;2](https://doi.org/10.1175/1520-0469(1995)052<1329:AMOTAS>2.0.CO;2).
- Hu, Q., and M. C. Veres, 2016: Atmospheric responses to North Atlantic SST anomalies in idealized experiments. Part II: North American precipitation. *J. Climate*, **29**, 659–671, <https://doi.org/10.1175/JCLI-D-14-00751.1>.
- Joshi, M. M., M. Stringer, K. Van der Wiel, A. O'Callaghan, and S. Fueglistaler, 2015: IGCMA: A fast, parallel and flexible intermediate climate model. *Geosci. Model Dev.*, **8**, 1157–1167, <https://doi.org/10.5194/gmd-8-1157-2015>.
- Kajtar, J. B., M. Collins, L. M. Frankcombe, M. H. England, T. J. Osborn, and M. Juniper, 2019: Global mean surface temperature response to large-scale patterns of variability in observations and CMIP5. *Geophys. Res. Lett.*, **46**, 2232–2241, <https://doi.org/10.1029/2018GL081462>.
- Keenlyside, N. S., J. Ba, J. Mecking, N. O. Omrani, M. Latif, R. Zhang, and R. Msadek, 2016: North Atlantic multi-decadal variability mechanisms and predictability. *Climate Change: Multidecadal and Beyond*, C.-P. Chang et al., Eds., World Scientific, 141–157.
- Kerr, R. A., 2000: A North Atlantic climate pacemaker for the centuries. *Science*, **288**, 1984–1985, <https://doi.org/10.1126/science.288.5473.1984>.
- Knight, J. R., R. J. Allan, C. K. Folland, M. Vellinga, and M. E. Mann, 2005: A signature of persistent natural thermohaline circulation cycles in observed climate. *Geophys. Res. Lett.*, **32**, L20708, <https://doi.org/10.1029/2005GL024233>.
- , C. K. Folland, and A. A. Scaife, 2006: Climate impacts of the Atlantic multidecadal oscillation. *Geophys. Res. Lett.*, **33**, L17706, <https://doi.org/10.1029/2006GL026242>.

- Knudsen, M. F., M.-S. Seidenkrantz, B. H. Jacobsen, and A. Kuijpers, 2011: Tracking the Atlantic multidecadal oscillation through the last 8,000 years. *Nat. Commun.*, **2**, 178, <https://doi.org/10.1038/ncomms1186>.
- Krishnamurthy, L., and V. Krishnamurthy, 2016: Teleconnections of Indian monsoon rainfall with AMO and Atlantic tripole. *Climate Dyn.*, **46**, 2269–2285, <https://doi.org/10.1007/s00382-015-2701-3>.
- Li, S., and G. T. Bates, 2007: Influence of the Atlantic multidecadal oscillation on the winter climate of East China. *Adv. Atmos. Sci.*, **24**, 126–135, <https://doi.org/10.1007/s00376-007-0126-6>.
- , and F.-F. Luo, 2013: Lead-lag connection of the Atlantic multidecadal oscillation (AMO) with East Asian surface air temperatures in instrumental records. *Atmos. Oceanic Sci. Lett.*, **6**, 138–143, <https://doi.org/10.1080/16742834.2013.11447070>.
- , J. Perlwitz, X. Quan, and M. P. Hoerling, 2008: Modelling the influence of North Atlantic multidecadal warmth on the Indian summer rainfall. *Geophys. Res. Lett.*, **35**, L05804, <https://doi.org/10.1029/2007GL032901>.
- , Y. Jing, and F. Luo, 2015: The potential connection between China surface air temperature and the Atlantic multidecadal oscillation (AMO) in the pre-industrial period. *Sci. China Earth Sci.*, **58**, 1814–1826, <https://doi.org/10.1007/s11430-015-5091-9>.
- Lin, J.-S., B. Wu, and T.-J. Zhou, 2016: Is the interdecadal circumglobal teleconnection pattern excited by the Atlantic multidecadal oscillation? *Atmos. Oceanic Sci. Lett.*, **9**, 451–457, <https://doi.org/10.1080/16742834.2016.1233800>.
- Liu, Y., and J. C. H. Chiang, 2012: Coordinated abrupt weakening of the Eurasian and North African monsoons in the 1960s and links to extratropical North Atlantic cooling. *J. Climate*, **25**, 3532–3548, <https://doi.org/10.1175/JCLI-D-11-00219.1>.
- Lu, R., B. Dong, and H. Ding, 2006: Impact of the Atlantic multidecadal oscillation on the Asian summer monsoon. *Geophys. Res. Lett.*, **33**, L24701, <https://doi.org/10.1029/2006GL027655>.
- Luo, F., S. Li, and T. Furevik, 2011: The connection between the Atlantic multidecadal oscillation and the Indian summer monsoon in Bergen Climate Model version 2.0. *J. Geophys. Res.*, **116**, D19117, <https://doi.org/10.1029/2011JD015848>.
- , —, Y. Gao, N. Keenlyside, L. Svendsen, and T. Furevik, 2018: The connection between the Atlantic multidecadal oscillation and the Indian summer monsoon in CMIP5 models. *Climate Dyn.*, **51**, 3023–3039, <https://doi.org/10.1007/s00382-017-4062-6>.
- McCabe, G. J., M. A. Palecki, and J. L. Betancourt, 2004: Pacific and Atlantic Ocean influences on multi-decadal drought frequency in the United States. *Proc. Natl. Acad. Sci. USA*, **101**, 4136–4141, <https://doi.org/10.1073/pnas.0306738101>.
- Monerie, P.-A., J. Robson, B. Dong, D. L. R. Hodson, and N. P. Klingaman, 2019: Effect of the Atlantic multidecadal variability on the global monsoon. *Geophys. Res. Lett.*, **46**, 1765–1775, <https://doi.org/10.1029/2018GL080903>.
- Msadek, R., and C. Frankignoul, 2009: Atlantic multidecadal oceanic variability and its influence on the atmosphere in a climate model. *Climate Dyn.*, **33**, 45–62, <https://doi.org/10.1007/s00382-008-0452-0>.
- , —, and L. Z. X. Li, 2011: Mechanisms of the atmospheric response to North Atlantic multidecadal variability: A model study. *Climate Dyn.*, **36**, 1255–1276, <https://doi.org/10.1007/s00382-010-0958-0>.
- O'Callaghan, A., M. Joshi, D. Stevens, and D. Mitchell, 2014: The effects of different sudden stratospheric warming types on the ocean. *Geophys. Res. Lett.*, **41**, 7739–7745, <https://doi.org/10.1002/2014GL062179>.
- Oglesby, R., S. Feng, Q. Hu, and C. Rowe, 2012: The role of the Atlantic multidecadal oscillation on medieval drought in North America: Synthesizing results from proxy data and climate models. *Global Planet. Change*, **84–85**, 56–65, <https://doi.org/10.1016/j.gloplacha.2011.07.005>.
- O'Reilly, C. H., L. Zanna, and T. Woollings, 2019: Assessing external and internal sources of Atlantic multidecadal variability using models, proxy data, and early instrumental indices. *J. Climate*, **32**, 7727–7745, <https://doi.org/10.1175/JCLI-D-19-0177.1>.
- Otterå, O. H., M. Bentsen, H. Drange, and L. Suo, 2010: External forcing as a metronome for Atlantic multidecadal variability. *Nat. Geosci.*, **3**, 688–694, <https://doi.org/10.1038/ngeo955>.
- Prasad, V. S., and T. Hayashi, 2005: Onset and withdrawal of Indian summer monsoon. *Geophys. Res. Lett.*, **32**, L20715, <https://doi.org/10.1029/2005GL023269>.
- Qian, C., J. Yu, and G. Chen, 2014: Decadal summer drought frequency in China: The increasing influence of the Atlantic multi-decadal oscillation. *Environ. Res. Lett.*, **9**, 124004, <https://doi.org/10.1088/1748-9326/9/12/124004>.
- Rasmusson, E. M., and T. H. Carpenter, 1982: Variations in tropical sea surface temperature and surface wind fields associated with the Southern Oscillation/El Niño. *Mon. Wea. Rev.*, **110**, 354–384, [https://doi.org/10.1175/1520-0493\(1982\)110<0354:VITSST>2.0.CO;2](https://doi.org/10.1175/1520-0493(1982)110<0354:VITSST>2.0.CO;2).
- Ratna, S. B., D. R. Sikka, M. Dalvi, and J. V. Ratnam, 2011: Dynamical simulation of Indian summer monsoon circulation, rainfall and its interannual variability using a high resolution atmospheric general circulation model. *Int. J. Climatol.*, **31**, 1927–1942, <https://doi.org/10.1002/joc.2202>.
- , T. J. Osborn, M. Joshi, B. Yang, and J. Wang, 2019: Identifying teleconnections and multidecadal variability of East Asian surface temperature during the last millennium in CMIP5 simulations. *Climate Past*, **15**, 1825–1844, <https://doi.org/10.5194/cp-15-1825-2019>.
- Schlesinger, M. E., and N. Ramankutty, 1994: An oscillation in the global climate system of period 65–70 years. *Nature*, **367**, 723–726, <https://doi.org/10.1038/367723a0>.
- Schubert, S. D., M. J. Suarez, P. J. Pegion, R. D. Koster, and J. T. Bacmeister, 2004: Causes of long-term drought in the US Great Plains. *J. Climate*, **17**, 485–503, [https://doi.org/10.1175/1520-0442\(2004\)017<0485:COLDIT>2.0.CO;2](https://doi.org/10.1175/1520-0442(2004)017<0485:COLDIT>2.0.CO;2).
- , and Coauthors, 2009: A U.S. CLIVAR project to assess and compare the responses of global climate models to drought-related SST forcing patterns: Overview and results. *J. Climate*, **22**, 5251–5272, <https://doi.org/10.1175/2009JCLI3060.1>.
- Si, D., and Y. Ding, 2016: Oceanic forcings of the interdecadal variability in East Asian summer rainfall. *J. Climate*, **29**, 7633–7649, <https://doi.org/10.1175/JCLI-D-15-0792.1>.
- Sikka, D. R., 1980: Some aspects of the large scale fluctuations of summer monsoon rainfall over India in relation to fluctuations in the planetary and regional scale circulation parameters. *J. Earth Syst. Sci.*, **89**, 179–195, <https://doi.org/10.1007/bf02913749>.
- , and S. B. Ratna, 2011: On improving the ability of a high resolution atmospheric general circulation model for dynamical seasonal prediction of the extreme seasons of the Indian summer monsoon. *Mausam*, **62**, 339–360.
- Slingo, J. M., 1987: The development and verification of a cloud prediction scheme for the ECMWF model. *Quart. J.*

- Roy. Meteor. Soc.*, **113**, 899–927, <https://doi.org/10.1002/qj.49711347710>.
- Soman, M. K., and K. K. Kumar, 1993: Space–time evolution of meteorological features associated with the onset of Indian summer monsoon. *Mon. Wea. Rev.*, **121**, 1177–1194, [https://doi.org/10.1175/1520-0493\(1993\)121<1177:STEOMF>2.0.CO;2](https://doi.org/10.1175/1520-0493(1993)121<1177:STEOMF>2.0.CO;2).
- Sun, C., F. Kucharski, J. Li, F. Jin, I. Kang, and R. Ding, 2017: Western tropical Pacific multidecadal variability forced by the Atlantic multidecadal oscillation. *Nat. Commun.*, **8**, 15998, <https://doi.org/10.1038/ncomms15998>.
- Sun, Y. B., S. C. Clemens, C. Morrill, X. Lin, X. Wang, and Z. An, 2012: Influence of Atlantic meridional overturning circulation on the East Asian winter monsoon. *Nat. Geosci.*, **5**, 46–49, <https://doi.org/10.1038/ngeo1326>.
- Sutton, R. T., and D. L. R. Hodson, 2005: Atlantic Ocean forcing of North American and European summer climate. *Science*, **309**, 115–118, <https://doi.org/10.1126/science.1109496>.
- Talento, S., T. J. Osborn, M. Joshi, S. B. Ratna, and J. Luterbacher, 2020: Response of the Asian summer monsoons to a high-latitude thermal forcing: Mechanisms and nonlinearities. *Climate Dyn.*, **54**, 3927–3944, <https://doi.org/10.1007/s00382-020-05210-9>.
- Ting, M. F., Y. Kushnir, R. Seager, and C. H. Li, 2011: Robust features of Atlantic multi-decadal variability and its climate impacts. *Geophys. Res. Lett.*, **38**, L17705, <https://doi.org/10.1029/2011GL048712>.
- Trenberth, K. E., D. P. Stepaniak, and J. M. Caron, 2000: The global monsoon as seen through the divergent atmospheric circulation. *J. Climate*, **13**, 3969–3993, [https://doi.org/10.1175/1520-0442\(2000\)013<3969:TGMAS>2.0.CO;2](https://doi.org/10.1175/1520-0442(2000)013<3969:TGMAS>2.0.CO;2).
- van der Wiel, K., A. J. Matthews, M. M. Joshi, and D. P. Stevens, 2016: Why the south Pacific convergence zone is diagonal? *Climate Dyn.*, **46**, 1683–1698, <https://doi.org/10.1007/s00382-015-2668-0>.
- Wang, B., and Z. Fan, 1999: Choice of South Asian summer monsoon indices. *Bull. Amer. Meteor. Soc.*, **80**, 629–638, [https://doi.org/10.1175/1520-0477\(1999\)080<0629:COSASM>2.0.CO;2](https://doi.org/10.1175/1520-0477(1999)080<0629:COSASM>2.0.CO;2).
- Wang, J., B. Yang, F. C. Ljungqvist, and Y. Zhao, 2013: The relationship between the Atlantic multidecadal oscillation and temperature variability in China during the last millennium. *J. Quat. Sci.*, **28**, 653–658, <https://doi.org/10.1002/jqs.2658>.
- , —, C. Qin, S. Kang, M. He, and Z. Wang, 2014: Tree-ring inferred annual mean temperature variations on the southern Tibetan Plateau during the last millennium and their relationships with the Atlantic multidecadal oscillation. *Climate Dyn.*, **43**, 627–640, <https://doi.org/10.1007/s00382-013-1802-0>.
- , —, F. C. Ljungqvist, J. Luterbacher, T. J. Osborn, K. R. Briffa, and E. Zorita, 2017: Internal and external forcing of multidecadal Atlantic climate variability over the past 1,200 years. *Nat. Geosci.*, **10**, 512–517, <https://doi.org/10.1038/ngeo2962>.
- Wang, Y., S. Li, and D. Luo, 2009: Seasonal response of Asian monsoonal climate to the Atlantic multidecadal oscillation. *J. Geophys. Res.*, **114**, D02112, <https://doi.org/10.1029/2008jd010929>.
- Webster, P. J., and S. Yang, 1992: Monsoon and ENSO: Selectively interactive systems. *Quart. J. Roy. Meteor. Soc.*, **118**, 877–926, <https://doi.org/10.1002/qj.49711850705>.
- Xia, J., Z. W. Yan, and P. L. Wu, 2013: Multidecadal variability in local growing season during 1901–2009. *Climate Dyn.*, **41**, 295–305, <https://doi.org/10.1007/s00382-012-1438-5>.
- , K. Tu, Z. Yan, and Y. Qi, 2016: The super-heat wave in eastern China during July–August 2013: A perspective of climate change. *Int. J. Climatol.*, **36**, 1291–1298, <https://doi.org/10.1002/joc.4424>.
- Zhang, L., and C. Wang, 2013: Multidecadal North Atlantic sea surface temperature and Atlantic meridional overturning circulation variability in CMIP5 historical simulations. *J. Geophys. Res.*, **118**, 5772–5791, <https://doi.org/10.1002/jgrc.20390>.
- Zhang, R., and T. L. Delworth, 2005: Simulated tropical response to a substantial weakening of the Atlantic thermohaline circulation. *J. Climate*, **18**, 1853–1860, <https://doi.org/10.1175/JCLI3460.1>.
- , and —, 2006: Impact of Atlantic multidecadal oscillations on India/Sahel rainfall and Atlantic hurricanes. *Geophys. Res. Lett.*, **33**, L17712, <https://doi.org/10.1029/2006GL026267>.
- Zhang, Z., X. Sun, and X.-Q. Yang, 2018: Understanding the interdecadal variability of East Asian summer monsoon precipitation: Joint influence of three oceanic signals. *J. Climate*, **31**, 5485–5506, <https://doi.org/10.1175/JCLI-D-17-0657.1>.
- Zhou, X. M., S. L. Li, F. Luo, Y. Gao, and T. Furevik, 2015: Air–sea coupling enhances East Asian winter climate response to the Atlantic multidecadal oscillation (AMO). *Adv. Atmos. Sci.*, **32**, 1647–1659, <https://doi.org/10.1007/s00376-015-5030-x>.
- Zhu, Y., T. Wang, and J. Ma, 2016: Influence of internal decadal variability on the summer rainfall in eastern China as simulated by CCSM4. *Adv. Atmos. Sci.*, **33**, 706–714, <https://doi.org/10.1007/s00376-016-5269-x>.